Kinetically Constrained Quantum Dynamics in Superconducting Circuits

Riccardo J. Valencia-Tortora,[1,*] Nicola Pancotti,[2,†] and Jamir Marino[1]

[1] *Institut für Physik, Johannes Gutenberg-Universität Mainz, Mainz D-55099, Germany*
[2] *AWS Center for Quantum Computing, Pasadena, California 91125, USA*

(Received 17 December 2021; accepted 5 May 2022; published 2 June 2022)

We study the dynamical properties of the bosonic quantum East model at low temperature. We show that a naive generalization of the corresponding spin-1/2 quantum East model does not possess analogous slow dynamical properties. In particular, conversely to the spin case, the bosonic ground state turns out to be *not* localized. We restore localization by introducing a repulsive interaction term. The bosonic nature of the model allows us to construct rich families of many-body localized states, including coherent, squeezed, and cat states. We formalize this finding by introducing a set of *superbosonic* creation-annihilation operators that satisfy the bosonic commutation relations and, when acting on the vacuum, create excitations that are exponentially localized around a certain site of the lattice. Given the constrained nature of the model, these states retain memory of their initial conditions for long times. Even in the presence of dissipation, we show that quantum information remains localized within decoherence times that are tunable with the parameters of the system. We propose an implementation of the bosonic quantum East model based on state-of-the-art superconducting circuits, which could be used in the near future to explore the dynamical properties of kinetically constrained models in modern platforms.

DOI: 10.1103/PRXQuantum.3.020346

I. INTRODUCTION

Robust storage of quantum information and decoherence induced by external baths are two important limiting factors that mitigate against a large-scale adoption of modern quantum technologies [1]. The storage of quantum information is a challenging task, as most interacting quantum systems tend to thermalize quickly. Once equilibrium is reached, the properties of the initial configurations are hard to retrieve, as they are ergodically scattered among exponentially many degrees of freedom [2]. In order to overcome this obstacle, many proposals have attempted to confine quantum information into conserved or quasiconserved quantities [3–19]. These proposals range from strongly disordered many-body localized [20,21] or glassy systems [22–29], in which thermalization is impeded by the presence of disordered potentials, to "fracton" systems, in which dynamical constraints induce fragmentation on the space of reachable configurations [30–37], and quantum scarred systems, in which certain classes of initial states show coherent oscillations for times longer than typical relaxation times [38–51]. Most of these phenomena often rely on such delicate properties that *any* weak coupling with an external environment could potentially become detrimental.

Quantum kinetically constrained models (KCMs) have recently attracted attention due to their distinctive dynamical properties. Motivated by the slowness of their classical counterparts, researchers have started to investigate their quantum generalizations, such as the quantum East model, the quantum Fredricksen-Andersen model, and others [52–58].

In this work, we explore the low-temperature dynamical properties of the bosonic quantum East model, a generalization of the spin-1/2 model studied in Refs. [26,59], in which spin excitations can only be created on sites to the "east" of a previously occupied one. Our contributions can be summarized as follows. (i) We show that repulsive density-density interactions are necessary to entail localization in the ground state, in contrast to East models with a finite-dimensional local Hilbert space. (ii) We exploit the properties of the localized phase and the bosonic nature of the model, to construct families of non-Gaussian many-body states that are useful for quantum-information processing. (iii) We illustrate how localization enhances the robustness of these states against decoherence. (iv) Finally, we propose an implementation of the bosonic quantum East model based on chains of superconducting qubits.

*Corresponding author. rvalenci@uni-mainz.de
†This work was done prior to joining Amazon

In the spin-1/2 case, evidence has been provided in support of a dynamical transition from a fast thermalizing regime to a slow nonergodic one [26,59]. In particular, in Ref. [59], it has been argued that the slow dynamics is a byproduct of the localized nature of the low-energy eigenstates of the model. Namely, the corresponding wave functions contain nontrivial excitations only on a small compact region of the lattice and they are in the vacuum state everywhere else. This has direct consequences for the dynamical properties of the system, as the localized states can be used as building blocks to construct exponentially many "slow" states in the size of the system.

The dynamical transition observed in Ref. [59] is not guaranteed to survive in the bosonic case. In fact, we provide strong numerical evidence that this is not the case for the most naive bosonic generalization of the spin-1/2 model. In order to restore localization at low temperature, we consider a modified model in which density-density interactions—absent in the bare spin case—play a crucial role. More precisely, we show that the ground state remains localized as we increase the finite cutoff of the local Fock-space dimension only in the presence of repulsive interactions. We support our findings by combining numerical and analytical approaches. Within the localized phase, the ground state is well approximated by a product state for any value of interaction. It is therefore well approximated by a matrix product state, making large system size and local Fock-space dimension numerically accessible (cf. Secs. II and III).

The bosonic generalization of the spin-1/2 East model opens up a number of directions, including the construction of many-body versions of archetypal states that are relevant for quantum-information applications such as coherent states, squeezed states, and cat states [60]. These states possess the same properties as their single-mode counterparts, although they are supported on a few neighboring sites. We provide a formal description of these objects by proposing a simple adiabatic protocol that defines a set of *superbosonic* creation-annihilation operators (Sec. IV). These operators fulfill the canonical bosonic commutation relations and they are exponentially localized in the neighborhood of a given site on the lattice. This allows us to construct an effective noninteracting theory at low temperature in terms of these operators, in which the Hamiltonian is reminiscent of the l-bit construction in many-body localization (MBL) [61–64].

In Sec. V, we couple the system to different noise sources and, via a detailed numerical analysis, we show that localized states retain some memory of their initial condition even in the presence of strong dissipation (see Fig. 1). First, we consider the effects of dephasing noise coupled to bosonic occupations, which preserves the "East symmetry" (see the definition in Sec. II). In this scenario, the localized states are barely altered by the environment. We show that the fidelity between the time-evolved state

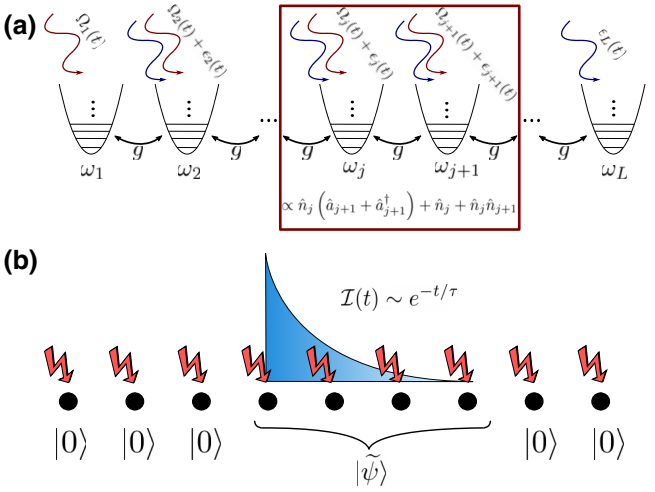

FIG. 1. (a) A chain of driven superconducting qubits coupled via exchange interaction g. In the red box, we write the low-energy effective interaction between the jth and $(j+1)$th superconducting qubits. (b) A sketch of a localized state subject to external noise (arrows). The visibility of the initial peak with respect to the rest of the system [measured by the imbalance $\mathcal{I}(t)$] decays exponentially with a time τ much larger than the characteristic operational time scales of state-of-the-art superconducting circuits.

and the initial state decays exponentially with a long decoherence time, controlled by the parameters of the Hamiltonian, the initial state, and the strength of the noise. Second, we consider the effects of particle losses that break the "East symmetry." As expected in this situation, the magnitude of the fidelity decays exponentially fast in time, with a decoherence time that is parametrically small in the loss rate. It is important to stress that as the localized states have nontrivial structure only on a small support, any external noise that does not act in their immediate vicinity leaves them essentially invariant. This set of noise-resilient properties renders the many-body states studied in this work qualitatively different from localization induced by disorder, which is inherently fragile to decoherence (for studies on MBL systems coupled to a bath or external noise, see Refs. [65–70]). In particular, in Sec. VI we argue that our localized states can be manipulated on time scales shorter than the characteristic relaxation and decoherence times of superconducting qubit wires.

In fact, our proposal for an implementation of the bosonic quantum East model based on superconducting qubits is one of the key findings of this work. In recent years, unprecedented quantum control of interacting superconducting qubits with microwave photons has been reached in circuit-QED platforms [71–79]. These circuits allow quantum-information-processing tasks and the quantum simulation of paradigmatic light-matter interfaces. Superconducting Josephson junctions allow us to introduce nonlinearity in quantum electrical circuits, which

is a key factor in protecting quantum resources, by making these platforms resilient to noise and errors. This is a key factor of merit for any superconducting qubit, ranging from the established transmon to, for instance, the more recently developed superconducting nonlinear asymmetric inductive element (SNAIL) [80,81]. Here, we consider a chain of superconducting qubits (see Refs. [80,82–89]), which can be described as anharmonic oscillators, coupled via a hopping term (cf. Fig. 1). In the limit of weak coupling and low anharmonicity, we find an effective description of such superconducting qubits array in terms of the bosonic quantum East chain.

The paper is organized as follows. In Sec. II, we introduce the Hamiltonian of the model, enumerate its symmetries, and compare it to previous works on similar models. In Sec. III, we explore the localization properties of the ground state of the model. In particular, we show when the transition point is independent of the size of the cutoff of the local Fock-space dimension and how the localization length behaves in the proximity of the transition. On the localized side of the transition, we quantitatively compare results extracted with tensor-network methods and mean field, and we show that they are in excellent agreement. In Sec. IV, we introduce a description in terms of superbosonic operators, which allows us to generalize coherent, squeezed, and cat states. In Sec. V, we study the robustness of these localized states against noise source. In Sec. VI, we present the implementation of the Hamiltonian for the bosonic quantum East model, based on a chain of superconducting qubits.

II. BOSONIC QUANTUM EAST MODEL

We investigate the following Hamiltonian with open boundary conditions:

$$H = -\frac{1}{2}\sum_{j=0}^{L}\hat{n}_j\left[e^{-s}\left(\hat{a}_{j+1}+\hat{a}_{j+1}^{\dagger}\right)-\epsilon\hat{n}_j-U\hat{n}_{j+1}-1\right], \tag{1}$$

where $\hat{a}_j$ and $\hat{a}_j^{\dagger}$ are bosonic annihilation and creation operators acting on site j, respectively; e^{-s} controls the constrained creation and annihilation of bosons; ϵ is the on-site density-density interaction; and U is the nearest-neighbor density-density interaction.

As discussed in Sec. I, Eq. (1) is a kinetically constrained "East" model. The unidirectional constrained feature has consequences for the accessible portion of the Hilbert space by the dynamics. Namely, any initial state with a product of vacua from the left edge up to a given site in the bulk will exhibit nontrivial dynamics only on the right side of the lattice after the first occupied site. For sake of concreteness, let us consider the state $|00100\ldots0\rangle$. Via subsequent application of the Hamiltonian given in Eq. (1), we have

$$\begin{array}{ccccc} & & & & |00120\ldots0\rangle\ldots \\ & & & \nearrow & \\ |00100\ldots0\rangle & \to & |00110\ldots0\rangle & \to & |001110\ldots0\rangle\ldots \\ & & & \searrow & \\ & & & & |00100\ldots0\rangle\ldots \end{array} \tag{2}$$

where $\to$ represents the action of the constrained creation and annihilation of bosons at each step of perturbation theory. The occupation of the first nonvacant site and of those at its left cannot change as a consequence of the "East" constraint. More formally, the Hamiltonian commutes with the projectors:

$$P(n_0,k) = \mathcal{P}_{0,j}^{\otimes_{j=0}^{k-1}}\otimes\mathcal{P}_{n_0,k}\otimes\mathbb{1}_j^{\otimes_{j>k}}, \tag{3}$$

where $\mathcal{P}_{s,j} = |s\rangle_{jj}\langle s|$ is the projector on the Fock state with s particles on site j, $\mathbb{1}_j$ is the identity acting on site j, and k and n_0 are, respectively, the position and occupation of the first nonvacant site. We can split the Hilbert space into dynamically disconnected sectors $\mathcal{H}_{n_0,k}$, such that the action of $P(n_0,k)$ is equivalent to the identity, while the action of the other projectors gives zero. For example, the state $|00100\ldots0\rangle \in \mathcal{H}_{1,2}$ (note that the first site index is 0). Furthermore, since $\sum_{k=0}^{L}\sum_{n_0=1}^{\infty}P(n_0,k)=\mathbb{1}$, these sectors $\{\mathcal{H}_{k,n_0}\}$ constitute a complete and orthogonal basis of the whole Hilbert space $\mathcal{H}$, namely $\mathcal{H}=\bigoplus_{k=0}^{L}\bigoplus_{n_0=1}^{\infty}\mathcal{H}_{n_0,k}$.

In the following, we focus on a certain block specified by k, n_0, and the number of "active" sites L right next to the kth one. Since the action of H on sites to the left of the kth one is trivial, the index k is physically irrelevant for our purpose and we therefore choose $k=0$ without any loss of generality. Exploiting this property, we write the Hamiltonian given in Eq. (1) as $H_{L+1}=\sum_{n_0}H_{L+1}(n_0)$, where $H_{L+1}(n_0)$ is

$$H_{L+1}(n_0) = \hat{h}_1 + \\ -\frac{1}{2}\sum_{j=1}^{L}\hat{n}_j\left[e^{-s}\left(\hat{a}_{j+1}+\hat{a}_{j+1}^{\dagger}\right)-\epsilon\hat{n}_j-U\hat{n}_{j+1}-1\right], \tag{4}$$

with $\hat{h}_1 \equiv -\frac{1}{2}n_0\left[e^{-s}\left(\hat{a}_1+\hat{a}_1^{\dagger}\right)-\epsilon n_0-U\hat{n}_1-1\right]$ and $n_0\in\mathbb{N}^+$. Furthermore, since $H_{L+1}(n_0)$ commutes with the operators acting on the $(L+1)$th site, we can represent it as the sum of an infinite number of commuting terms $H_{L+1}(n_0)=\sum_{\beta_r}H_L^{\beta_r}(n_0)\otimes\Pi_{L+1}^{\beta_r}$, where Π_L^{β} is the projector over the eigenstate $|\beta_r\rangle$ with eigenvalue

$\beta_r = rU - e^{-2s}/U$ of the operator $\left(U\hat{n}_{L+1} - e^{-s}\left(\hat{a}_{L+1} + \hat{a}^\dagger_{L+1}\right)\right)$, where $r \in \mathbb{N}$, and

$$H_L^{\beta_r}(n_0) = \hat{h}_1 + - \frac{1}{2}\sum_{j=1}^{L-1} \hat{n}_j \left[e^{-s}\left(\hat{a}_{j+1} + \hat{a}^\dagger_{j+1}\right) - \epsilon\hat{n}_j - U\hat{n}_{j+1} - 1\right] + \frac{1}{2}\hat{n}_L\left[\beta_r + \epsilon\hat{n}_L + 1\right]. \quad (5)$$

In Sec. III, we focus on the properties of the ground state of the Hamiltonian given in Eq. (5) within a certain symmetry sector.

The Hamiltonian given in Eq. (1) can be linked to its spin-1/2 version [59] by setting $U = \epsilon = 0$ and replacing the bosons with hard-core ones. Since the Hilbert space of each spin is finite, the "East" symmetry is largely reduced with respect to the bosonic case. Each symmetry sector $\mathcal{H}_{k,n_0=1}$ is specified only by the position of the first excitation, since n_0 is bound to be zero or one. The ground-state properties within a symmetry sector $\mathcal{H}_{k,n_0=1}$, where the position k of the first nonempty site is again irrelevant, have been investigated in Ref. [59]. It has been observed that the probability of finding an occupied site in the ground state decays exponentially fast around the first occupied site when $s > 0$, namely

$$\langle \hat{n}_j \rangle \sim \exp[-j/\xi(s)], \quad (6)$$

where the expectation value is taken on the ground state and we introduce the localization length $\xi > 0$. The localization length ξ is the typical distance from the first occupied site such that the state becomes a trivial product state that is well approximated by the vacuum.

In Sec. III, we investigate the conditions for localization of the ground state at finite values of s upon trading spins (hard-core bosons) for bosons. Such generalization is not taken for granted. The amplitude for "eastern" particle creation can now be enhanced by the prefactor n_0, suggesting that the transition may be qualitatively established when $(n_0 e^{-s}) \sim 1$. This would imply a critical value $s_c \propto \log n_0$, which is parametrically large in n_0, pushing the extension of the localized phase up to $s \to \infty$. Nonetheless, we show in Sec. III that a localized phase still occurs for $s > 0$ whenever repulsive interactions are included in Eq. (1).

III. LOCALIZATION TRANSITION

In this section, we show that the Hamiltonian in Eq. (5) displays a localization-delocalization transition at finite s and $U > 0$. We give numerical evidence corroborated by analytical observations that repulsive interactions are necessary to observe such a transition at finite s. We use the inverse localization length ξ^{-1} controlling the decay of the average occupation number in space [cf. Eq. (6)] as a proxy for the transition.

In the following, we fix $\epsilon = 0$ and the symmetry sector $\beta_{r=0}$ in Eq. (5), unless mentioned otherwise. The additional nonlinear term proportional to ϵ would complicate the analysis from a technical standpoint without altering the main contents of the paper. For the sake of clarity, Appendix A shows that, for $U = 0$ and $\epsilon > 0$, the localization properties of the ground state remain qualitatively similar to those discussed in the main text.

In order to investigate the properties of the ground state, we resort to a combination of mean-field arguments, exact diagonalization (ED), and density matrix renormalization group (DMRG) methods [90]. Since we aim to explore large system sizes, we mainly resort to the DMRG and we use ED as a benchmark when both methods can be used. Interestingly, we find that mean field is able to analytically predict the location of the transition point obtained via the DMRG.

We compute the ground state $|\psi_0(n_0)\rangle$ at fixed n_0, s, and U. We fix the system size at $L = 15$. This value is sufficiently large to capture the localized tail of the ground state, without relevant finite-size effects. Although the local Fock space is infinite, in order to treat the model numerically, we need to fix a finite cutoff Λ. We work with Fock states $|0\rangle$ through $|\Lambda\rangle$, such that the spin-1/2 case of Ref. [59] is recovered at $\Lambda = 1$. In Appendix B, we show how localization is only mildly dependent on the sector selected by the occupation n_0 of the zeroth site. Accordingly, in the following, we set $n_0 = 1$.

The Hamiltonian is one dimensional, local, and gapped at finite Λ; therefore, its ground state can be efficiently accessed via a matrix product state (MPS) formulation of the DMRG [90]. The main source of error is given by the finite cutoff Λ. Indeed, the properties of $|\psi_0(n_0)\rangle$ can change nontrivially as a function of Λ. More precisely, for any finite cutoff Λ, the model falls into the class of localized systems studied in Ref. [59]. As a result, $|\psi_0(n_0)\rangle$ is always localized for a large enough s at finite Λ but this does not imply localization for $\Lambda \to \infty$. Indeed, although $U > 0$ makes the spectrum of the Hamiltonian in Eq. (1) bounded from below, it does not ensure that its ground state is still localized in space when s is finite. In the following, we extract the $\Lambda \to \infty$ limit via a scaling analysis.

In Fig. 2, we show the average occupation number $\langle \hat{n}_j \rangle$ as a function of site j for some values of s at fixed $U = 1$. For s not large enough, the average occupation does not change smoothly with the site j and it saturates the cutoff Λ, meaning that there are strong finite-cutoff effects. In contrast, for s large enough, the occupation decays exponentially in j, matches Eq. (6) well, and does not change upon increasing the cutoff Λ. The value of s at which this change of behavior occurs depends on U, as we discuss in more detail in this section.

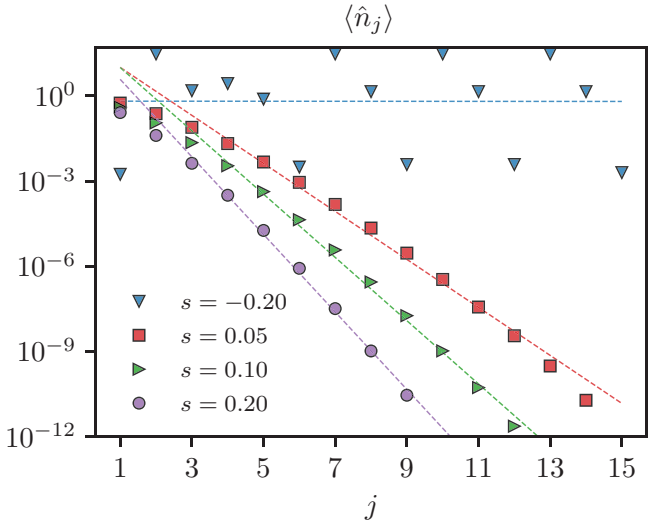

FIG. 2. The average occupation number of the ground state for different values of s at fixed nearest-neighbor density interaction $U = 1$. We fix $L = 15$, a cutoff $\Lambda = 30$ to the maximal occupation number, and $n_0 = 1$. In the plot, we do not display the occupation n_0 of the zeroth site that fixes the "East symmetry" sector. The dashed lines are the exponential fit, the slope of which is $-1/\xi$, where ξ is the localization length [cf. Eq. (6)].

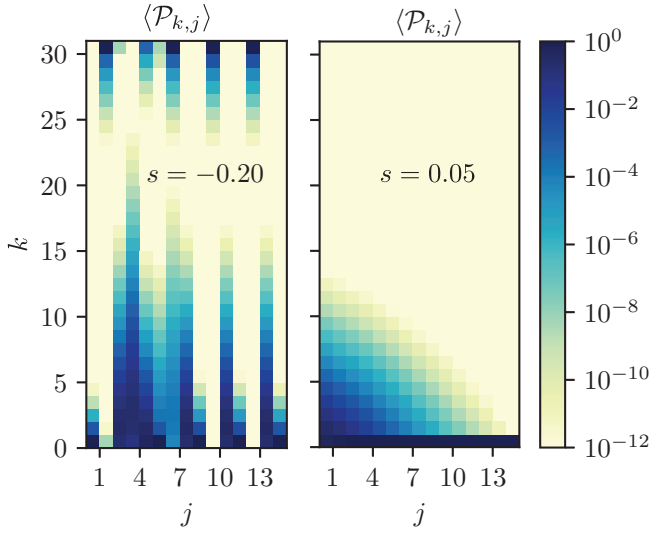

FIG. 3. The probability of having $k \in [0, \Lambda]$ bosons on site $j \in [1, L]$ in the ground state. In the plot, we do not display the occupation n_0 of the zeroth site that fixes the "East symmetry" sector. We fix $L = 15$, $\Lambda = 30$, $n_0 = 1$, and $U = 1$. In the left panel, we consider a typical configuration in the delocalized phase ($s = -0.20$). The cutoff is saturated over many sites. The staggered feature is due to the repulsive nearest-neighbor interaction. In the right panel, we consider a typical localized ground state ($s = 0.05$). Along each site j, the probability of having k bosons, $\langle \mathcal{P}_{kj} \rangle$, drops exponentially fast with k. The light color means that the value is smaller than 10^{-12}.

In order to check the effects of a finite Λ cutoff, we compute the probability of having k bosons on site j, namely the expectation value of the projector $\mathcal{P}_{kj} = |k\rangle_{jj}\langle k|$, where $|k\rangle_j$ is the Fock state with k particles on site j. In Fig. 3, we show $\langle \mathcal{P}_{kj} \rangle$ as a function of k and j for typical localized and delocalized ground states, respectively. The results in the delocalized phase are not reliable, since the observable suffers finite-cutoff effects. Instead, in the localized phase,

$$\langle \mathcal{P}_{kj} \rangle \sim e^{-k/\xi_{Fj}}, \tag{7}$$

with $\xi_{Fj} > 0$ for any site j. The exponential decay in the localized phase sheds additional light on the fact that the system is well described by a finite effective cutoff (for additional details, see Appendix C).

For each value of U and Λ, the inverse of the localization length goes from values smaller than or equal to zero to positive values as s increases. We identify the region where $1/\xi \leq 0$ as the delocalized phase, while the region where $1/\xi > 0$ is identified as the localized phase. In the delocalized phase, strong finite cutoff effects can lead to a positive localization length ξ. In order not to mistakenly identify these points as belonging to the localized phase, we fix a threshold $\lambda > 0$ and for each Λ and U we identify the transition point $s_c(U, \Lambda)$ as the value of s such that $1/\xi \leq \lambda$ and $1/\xi > \lambda$ for s smaller and greater than $s_c(U, \Lambda)$, respectively. We choose $\lambda \approx 10^{-1}$. The results are weakly affected by this choice of λ. Furthermore, the precise location of the transition point $s_c(U, \Lambda)$ is beyond the scope of this work, since we are interested in engineering states deep in the localized phase, as we discuss extensively in Sec. IV.

As discussed above, in the delocalized phase, results are strongly dependent on the cutoff, since the average occupations always saturate their artificial upper bound. This circumstance allows us to draw only qualitative conclusions on the physics at $s < s_c$ in the case of the bosonic East model ($\Lambda \to \infty$).

In Fig. 4, we show the inverse of the localization length ξ swiping s for different values of Λ at fixed U. For $U = 0$, the transition point $s_c(U = 0, \Lambda)$ always increases with Λ. Instead, when $U > 0$, the transition point converges to a finite value independent of Λ for $\Lambda \to \infty$. In the inset of Fig. 4, we show the numerically extracted transition point $s_c(U, \Lambda)$ as a function of Λ and U. For $U > 0$, it is possible to extract a finite value of $s_c(U) \equiv \lim_{\Lambda\to\infty} s_c(U, \Lambda)$. Instead, for $U = 0$, the transition point scales as $s_c(U = 0, \Lambda) \propto \log(\Lambda)$, suggesting that in the actual bosonic system we have $s_c(U = 0) = \infty$, meaning that there is no transition. Therefore, whenever $U > 0$, the system undergoes a delocalized-localized transition at finite $s_c(U)$. In Fig. 5, we show the inverse of the localization length ξ as a function of s for different values of U at fixed Λ. The transition point s_c depends on the competition between the dynamical term, controlled by e^{-s}, and the nearest-neighbor density term, proportional to U. The former

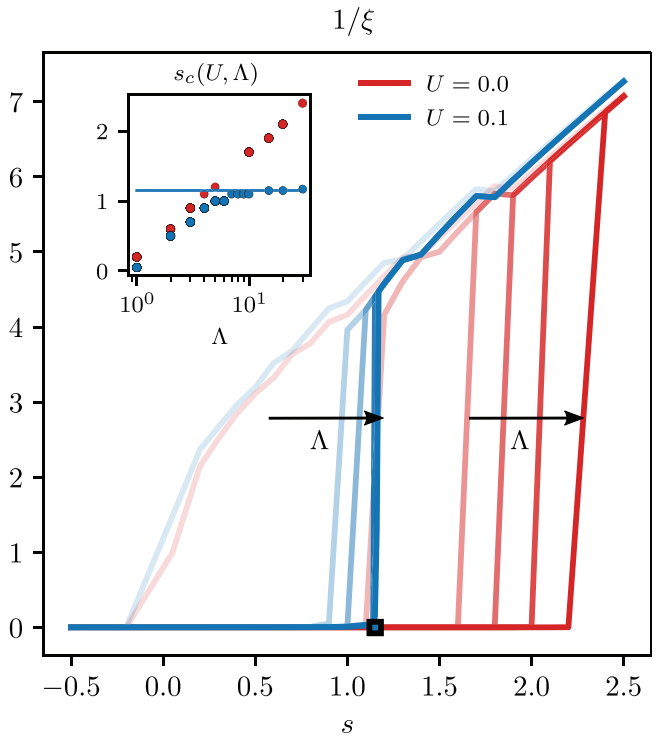

FIG. 4. The inverse of the localization length ξ in a system of $L = 15$ "active" sites in the symmetry sector $n_0 = 1$ and $\beta_{r=0}$. The main plot shows the inverse of the localization length ξ^{-1} as a function of s for different values of $\Lambda \in [1, 30]$ and U. The darker lines correspond to larger values of Λ. The square is the mean-field estimate of s_c in the bosonic case ($\Lambda = \infty$). The inset shows the behavior of $s_c(U, \Lambda)$ as a function of Λ for $U = 0$ (red) and $U = 0.1$ (blue). The circles correspond to numerically extracted values from the DMRG results, while the continuous lines are the mean-field estimate $s_c \approx \log(1/\sqrt{U})$, which matches the numerics at large Λ.

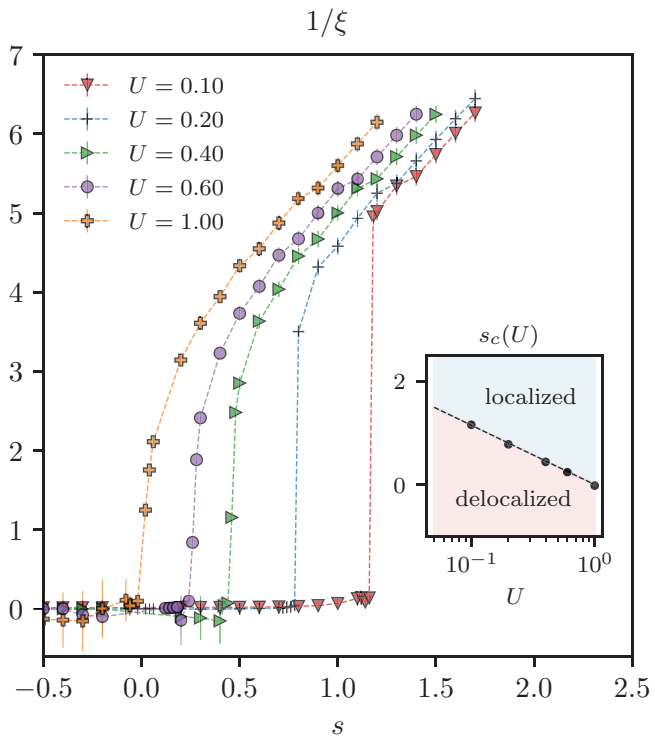

FIG. 5. The inverse of the localization length ξ in a system of $L = 15$ "active" sites in the symmetry sector $n_0 = 1$ and $\beta_{r=0}$. We fix the cutoff $\Lambda = 30$. The main plot shows the inverse of the localization length ξ^{-1} as a function of s for different values of U. We plot the error bars on top of each point. In the inset, we plot the transition point $s_c(U)$ as a function of U. The dots represent the extracted $s_c(U) \equiv \lim_{\Lambda\to\infty} s_c(U, \Lambda)$. The dashed line is the mean-field estimate for the transition point $s_c^{MF}(U) = \log(1/\sqrt{U})$.

favors the delocalization of the state, while the latter favors its localization. Indeed, in the $U \to 0$ limit, we provide evidence that the bosonic system is always delocalized if $s < \infty$. Instead, in the large-U limit, the Hamiltonian is approximated by $U\sum_i \hat{n}_i\hat{n}_{i+1} + \hat{n}_i$, the ground state of which in a specific symmetry sector at given total particle number is simply $|n_0\rangle|00\ldots0\rangle$.

The role of the interaction term U in the localization of the bosonic system can be appreciated in a mean-field treatment. We project the Hamiltonian into the manifold of coherent product states $|\phi\rangle = \bigotimes_{j=1}^{L} |\alpha_j\rangle_j$, with $\hat{a}_j|\alpha_j\rangle_j = \alpha_j|\alpha_j\rangle_j$. We evaluate the Hamiltonian given in Eq. (4) in this basis:

$$\langle\phi|H(n_0)|\phi\rangle = -\frac{1}{2}\sum_{j=0}^{L} |\alpha_j|^2 \left(2e^{-s}\alpha_{j+1} - U|\alpha_{j+1}|^2 - 1\right), \tag{8}$$

where $|\alpha_j|^2$ is the average number of particles in the coherent state at site j. From unidirectionality of the interaction, we can write $\langle\phi|H(n_0)|\phi\rangle = -\frac{1}{2}\sum_j |\alpha_j|^2 h_j(\alpha_{j+1}, s, U)$, where $h_j(\alpha_{j+1}, s, U) = \left(2e^{-s}\alpha_{j+1} - U|\alpha_{j+1}$ For energetic stability the effective field $h_j(\alpha_{j+1}, s, U)$ on site, j should be negative:

$$\left(2e^{-s}\alpha_{j+1} - U|\alpha_{j+1}|^2 - 1\right) < 0 \Rightarrow$$
$$\Rightarrow s > \log\left(\frac{2\alpha_{j+1}}{1 + U|\alpha_{j+1}|^2}\right) \equiv s_c(\alpha_{j+1}). \tag{9}$$

Since the system does not conserve the number of particles, there can be an unbounded number of excitations in the ground state within a fixed-symmetry sector. Therefore, in order to have localization at a mean-field level, it is necessary that Eq. (9) holds for any value of $\alpha_{j+1} \in [0, \infty)$, namely $s > \max_{\alpha_{j+1}} s_c(\alpha_{j+1})$, and for all sites. For $U > 0$, such a condition is satisfied if $s > \log(1/\sqrt{U})$, which turns to be in very good agreement with the DMRG numerical findings (see Fig. 5). Instead, for $U \leq 0$, there is no finite value of s that fulfills Eq. (9) for all α_{j+1}.

The excellent agreement between the DMRG and the mean-field analysis can be explained by observing that the ground state $|\psi_0\rangle$ (excluding the zeroth site, which fixes

the symmetry sector) obtained via the DMRG is well approximated via a product state, namely $|\psi_0\rangle \approx \bigotimes_{j=1}^{L} |\phi_j\rangle$. To further investigate the nature of the state $|\psi_0\rangle$, we consider the correlator $\Delta_j \equiv (\langle \hat{n}_j \hat{n}_{j+1}\rangle - \langle \hat{n}_j\rangle\langle \hat{n}_{j+1}\rangle)$. We use this operator as a proxy for non-Gaussian correlations. We compare Δ_j computed on the ground state obtained via the DMRG and the one computed assuming that the same state is Gaussian in the operators $\{\hat{a}_j^{(\dagger)}\}_{j=1}^{L}$, using Wick's theorem. As shown in Appendix D, the closer we are to the transition point s_c, the more the state develops non-Gaussian features at distances $j \lesssim \xi$. On the contrary, deep in the localized phase, the Gaussian ansatz captures the actual correlations at all sites well. Indeed, in the large-s limit, the Hamiltonian turns out to be diagonal in the number basis, namely $H(s \gg 1) \sim \sum_j (\hat{n}_j \hat{n}_{j+1} + \hat{n}_j)$, the ground state of which is $|n_0\rangle|00\ldots0\rangle$, which is a product state of Gaussian states (excluding the zeroth site, which fixes the symmetry sector).

The localized tail can be explained in a more intuitive way via the adiabatic theorem. Indeed, the Hamiltonian is gapped in the localized phase when $U > 0$; therefore, we can adiabatically connect two ground states within it. In particular, we can link any localized ground state to the one at $s = \infty$. This choice is particularly convenient since the Hamiltonian is diagonal in the number basis at $s = \infty$, $H(s \to \infty) = \sum_{j=1}(U\hat{n}_j\hat{n}_{j+1} + \hat{n}_j)/2$ and its ground state at the fixed-symmetry sector is simply $|n_0\rangle \bigotimes_{j=1}^{L} |0\rangle_j$. Then, the evolution with the adiabatically changing Hamiltonian will dress the initial site with an exponentially localized tail. In Sec. IV, we further exploit the adiabatic theorem to design the many-body version of a variety of states that are relevant in quantum-information setups, such as coherent states, cat states, and squeezed states.

IV. LOCALIZED-STATE ENGINEERING

In Sec. III, we have discussed the localization properties of the ground state of the bosonic quantum East model within each symmetry sector specified by the occupation n_0 of the first nonvacant site. In this section, we show that the ground states of different symmetry sectors are connected via bosonic creation and annihilation operators. We use this infinite set of localized states to construct the localized versions of cat, coherent, and squeezed states that are relevant for quantum-information purposes. These states share the same properties as their single-mode counterparts, although they are supported on a few neighboring sites toward the East as the ground states.

Starting with a given symmetry sector fixed by n_0, our aim is to find operators $\mathcal{A}$ and $\mathcal{A}^\dagger$ that obey the bosonic canonical commutation relations $[\mathcal{A}, \mathcal{A}^\dagger] = 1$, with the defining property

$$\left(\mathcal{A}^\dagger\right)^{n_0} |0\rangle = \mathcal{N}|n_0\rangle \otimes |\psi_0(n_0)\rangle := \mathcal{N}|\widetilde{n}_0\rangle, \qquad (10)$$

where $|\psi_0(n_0)\rangle$ is the localized tail of the ground state at fixed-symmetry sector n_0 and $\mathcal{N}$ is a constant. In other words, by acting n_0 times on the bosonic vacuum state with the operator $\mathcal{A}^\dagger$, we aim to retrieve the localized ground state of the Hamiltonian in Eq. (1) in the symmetry sector with n_0 particles on the first nonvacant site. From now on, we refer to these operators as *superbosonic* creation and annihilation operators since, in contrast to single site annihilation and creation operators, they act on a localized region of the system, by creating or destroying a bosonic localized tail along the chain. Likewise, we refer to the localized ground states $|\widetilde{n}_0\rangle$ as *superbosons*.

In order to find an explicit form for such operators, we employ the adiabatic theorem. From numerical evidence, our Hamiltonian is gapped within the whole localized phase (see Fig. 6). Therefore, there exists a slow tuning of s that enables us to connect two localized ground states at fixed values of U and n_0. We consider such a unitary transformation $\mathcal{U}(s, U)$ linking the ground state for $s = \infty$ with the target one at $s > s_c(U)$ in a fixed-symmetry sector specified by the occupation n_0 of the first nonvacant site. We fix $s = \infty$ as our starting point since the Hamiltonian is diagonal in the number operator when $s \to \infty$ and its ground state is simply the tensor product $|n_0\rangle \otimes_{j\geq 1} |0\rangle_j$. By the adiabatic theorem, the unitary operator takes the

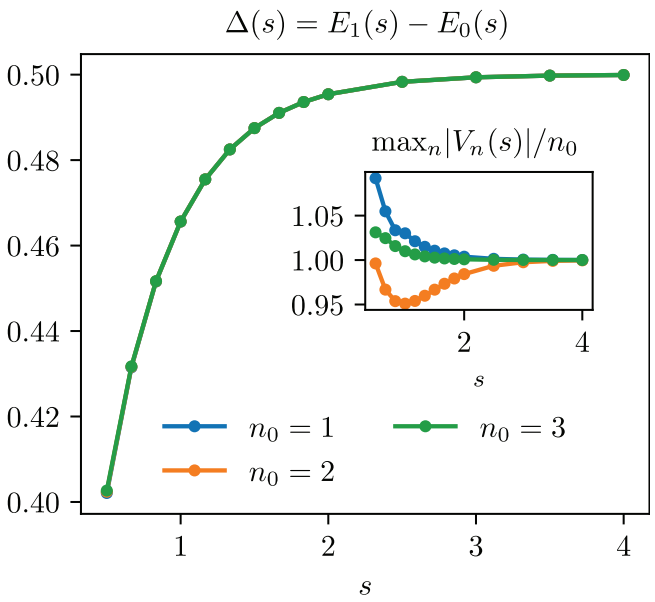

FIG. 6. The gap of the Hamiltonian in Eq. (5) as a function of $s \in [0.5, 4]$ for different values of the occupation n_0 of the first nonempty site. The inset shows the maximum matrix element $\max_n V_n(s)/n_0 \equiv \max_n \langle\psi_n(s)|V|\psi_0(s)\rangle/n_0$ of the perturbation $V = \sum_j \hat{n}_j (\hat{a}_{j+1} + \hat{a}_{j+1}^\dagger)$ between the nth excited state and the ground state at fixed s. We fix a system size $L = 6$, cutoff $\Lambda = 3$, and nearest-neighbor density-density interaction $U = 1$. The transition point is at $s_c(U = 1) \approx 0$. The results are weakly affected (of the order of few percent) by the finite cutoff Λ for $s \lesssim 2$.

following form [91,92]:

$$\mathcal{U}(s,U)=\mathcal{T}\exp\left[-i\int_0^T dtH\left(s(t)\right)\right], \tag{11}$$

where $\mathcal{T}$ indicates the time-ordering operator and $s(t)$ is a function that interpolates from $s(t=0)=\infty$ and $s(t=T)=s$. The function $s(t)$ has to be chosen such that it satisfies [91,92],

$$\frac{1}{\Delta(t)^2}\max_{n\neq 0}\left|\langle\Psi_n(t)|\dot{H}(t)|\Psi_0(t)\rangle\right|\ll 1, \tag{12}$$

at all times t. In Eq. (12), the state $|\Psi_n(t)\rangle$ is the nth excited eigenstate of the Hamiltonian computed at time t; $\dot{H}(t)$ is the time derivative of the Hamiltonian, which encodes the information about the specific protocol; and, finally, $\Delta(t)\equiv E_1(t)-E_0(t)$ is the gap at time t. For a reasonably fast protocol, we require $\Delta(s)\sim\mathcal{O}(1)$ in the parameter regime of interest. We write $H[s(t)]=H(s=\infty)+J(t)V$, where $H(s=\infty)=\sum_j(\hat{n}_j+U\hat{n}_j\hat{n}_{j+1})/2$, and $V=\sum_j\hat{n}_j(\hat{a}_{j+1}+\hat{a}_{j+1}^\dagger)$ is the coupling that we adiabatically switch on through the time-dependent protocol $J(t)=-e^{-s(t)}/2$. The time derivative of the Hamiltonian then reads $\dot{H}(t)=\dot{J}(t)V$. Let us focus on the perturbation V and the gap Δ at first and then on the specific protocol $J(t)$. In Fig. 6, we show the gap of the Hamiltonian and the maximum matrix element $\max_n V_n(s)\equiv\langle\psi_n(s)|V|\psi_0(s)\rangle$ connecting the ground to the nth excited state as a function of s at fixed U. Within the localized phase, the gap is $\mathcal{O}(1)$ and the maximum matrix element $\max_n V_n(s)\sim n_0$, where n_0 is the occupation of the first nonempty site fixing the symmetry sector. Due to the kinetic constraint, the largest matrix element $\max_n V_n(s)$ is between the localized ground state and the second localized state perturbatively close to the product states $|n_0100\ldots\rangle$ (note that this is not necessarily the first excited state). Therefore, the leading contribution comes from the first few sites, since the other terms are exponentially suppressed in the localization length of $|\Psi_0\rangle$. Let us consider, as a possible adiabatic protocol, the linear ramping $J(t)=-e^{-s}t/(2T)$, where $t\in[0,T]$, with T as the total duration time. From Eq. (12), the total time T has to satisfy $T\gg n_0e^{-s}$. Recall that we set the on-site bare frequency of the bosons as our energy scale and therefore the time T is expressed in that unit as well. In Sec. VI, we propose a possible experimental implementation of the bosonic quantum East model based on superconducting qubits. The typical on-site bare frequency of superconducting qubits is $\mathcal{O}$(GHz), leading to $T\gg(n_0e^{-s})$ns $\sim$ 1ns, which is within the typical coherence time of $\mathcal{O}(1\ \mu$s) of state-of-the-art superconducting qubits [71].

For $s(t)$ that satisfies Eq. (12), we obtain

$$\mathcal{U}(s,U)|n_0\rangle_0\bigotimes_{j=1}^{L}|0\rangle=e^{i\theta}|\widetilde{n}_0\rangle, \tag{13}$$

where θ is a phase acquired during the adiabatic time evolution [91,92]. Using $|n_0\rangle_0=\left(\hat{a}_0^\dagger\right)^{n_0}|0\rangle/\sqrt{n_0!}$ and $\mathcal{U}(s,U)|00\ldots0\rangle=|00\ldots0\rangle$, we obtain

$$\left(\mathcal{A}(s,U)^\dagger\right)^{n_0}|\widetilde{0}\rangle=e^{i\theta}\sqrt{n_0!}|\widetilde{n}_0\rangle, \tag{14}$$

where $|\widetilde{0}\rangle\equiv|00\ldots0\rangle$ and $\mathcal{A}(s,U)^\dagger=\mathcal{U}(s,U)\hat{a}_0^\dagger\mathcal{U}(s,U)^\dagger$. We can straightforwardly generalize Eq. (14) taking into account the position j starting from which we want to embed the state $|\widetilde{n}_0\rangle$. We define $\mathcal{A}_j(s,U)^\dagger=\mathcal{U}(s,U)\hat{a}_j^\dagger\mathcal{U}(s,U)^\dagger$, the action n_0 times of which on the bosonic vacuum generates the state $|0\rangle_\ell^{\otimes_{\ell<j}}\otimes|\widetilde{n}_0\rangle$. Differently from the generic interacting case, the dressed operator $\mathcal{A}_j^{(\dagger)}(s,U)$ acts nontrivially in a region exponentially localized around j. The operator $\mathcal{A}_j(s,U)^{(\dagger)}$ satisfies the bosonic commutation relations, since they are connected via a unitary transform to the bare bosonic operators $\hat{a}_j^{(\dagger)}$. Therefore, they are bosonic operators. As anticipated, we call the operators $\mathcal{A}_j(s,U)^{(\dagger)}$ *superbosonic* annihilation(creation) operators.

Since the transition point s_c is essentially independent of the value of n_0 (see Appendix B), we can design a protocol that obeys the adiabatic theorem for any initial state $|n_0\rangle\otimes|0\ldots0\rangle$. Furthermore, since these states belong to dynamically disconnected symmetry sectors, $\mathcal{H}_{k=0,n_0}$, for any values of s and U, it is possible to adiabatically evolve them independently of each other. Therefore, any linear combination of initial states turns under the adiabatic protocol into

$$\begin{aligned}\mathcal{U}(s,U)\sum_{n_0}c_{n_0}|n_0\rangle\otimes|0\ldots0\rangle&=\sum_{n_0}c_{n_0}\left(\mathcal{A}(s,u)^\dagger\right)^{n_0}|\widetilde{0}\rangle\\&=\sum_{n_0}c_{n_0}e^{i\theta(n_0,s,U,T)}|\widetilde{n}_0\rangle,\end{aligned} \tag{15}$$

where $\theta(n_0,s,U,T)$ is the phase acquired during the adiabatic time evolution. As discussed in Appendix B, deep in the localized phase the spectrum depends linearly on n_0, with small corrections. Since the phase acquired during the adiabatic evolution depends on the energy of the given state during the protocol, we have $\theta(n_0,s,U,T)\sim n_0f(s,U,T)$, where $f(s,U,T)$ is a function that is dependent on the specific protocol. This has important consequences for the state engineering that we discuss in the following. As an example, let us consider as initial

state of the adiabatic preparation the coherent state $|\alpha\rangle \equiv |\alpha\rangle_0 \bigotimes_{j\geq 1} |0\rangle_j$, where

$$|\alpha\rangle_0 = \sum_{n=0}^{\infty} \frac{e^{-|\alpha|^2/2}\alpha^n}{\sqrt{n!}} |n\rangle_0. \tag{16}$$

Using Eq. (15), the state $|\alpha\rangle$ turns into

$$\begin{aligned}\mathcal{U}(s,U)|\alpha\rangle &= \sum_{n=0}^{\infty} \frac{e^{-|\alpha|^2/2}\alpha^n}{\sqrt{n!}} e^{i\theta(n,s,U,T)} |\widetilde{n}\rangle \\ &= \sum_{n=0}^{\infty} \frac{e^{-|\alpha'|^2/2}\alpha'^n}{\sqrt{n!}} |\widetilde{n}\rangle,\end{aligned} \tag{17}$$

where $\alpha' = \alpha e^{if\,(s,U,T)}$. In Fig. 7, we compute the overlap between $\mathcal{U}(s(t),U)|\alpha\rangle$ and the *superbosons* $|\widetilde{n}(s(t),U)\rangle$ for different values of α at the initial time $t=0$ and at the final time $t=T$ of the adiabatic transformation. At the initial time, we have $\mathcal{U}(s(0),U)|\alpha\rangle = |\alpha\rangle$ and $|\widetilde{n}(s(0),U)\rangle = |n\rangle \otimes |00\ldots0\rangle$. At the final time, we have $|\widetilde{n}(s(T),U)\rangle = |\widetilde{n}\rangle$. In Fig. 7, the overlaps are in very good agreement with Eq. (17) and we obtain the desired state in Eq. (17) with a fidelity ≈ 0.9994 for $\alpha = 1.5$. We expect that when α is large, the fidelity achieved by the protocol becomes small, since corrections to the linear dependence of $\theta(n,s,U,T)$ from n become important. We call the localized version of a coherent state $|\widetilde{\alpha}\rangle \equiv \mathcal{U}(s,U)|\alpha\rangle$ a *supercoherent* state.

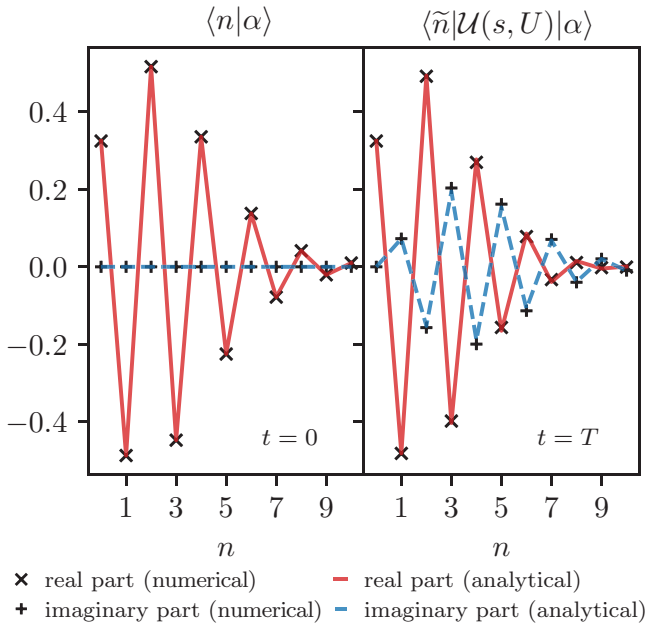

FIG. 7. At $t=0$, the system is prepared in a single-body coherent state $|\alpha\rangle = |\alpha\rangle_0 \bigotimes_{j=1}^{L} |0\rangle_j$, where $|\alpha\rangle_0$ is a coherent state on the first site with $\alpha = 1.5$. At time $t \geq 0$, we apply the adiabatic protocol defined in Eq. (11) to the state $|\alpha\rangle$ up to time $t=T$, obtaining $|\widetilde{\alpha}'\rangle$. In the left panel, we compute the probability amplitudes $\langle n|\alpha\rangle$, where $|n\rangle = |n\rangle_0 \bigotimes_{j=1}^{L} |0\rangle_j$ is an eigenstate of the number operator $\hat{n}_0$. The data (symbols) match the amplitudes of a single-site coherent state with $\alpha = 1.5$ (continuous and dashed line). In the right panel, we compute the probability amplitudes $\langle\widetilde{n}|\mathcal{U}(s,U)|\alpha\rangle$, where $|\widetilde{n}\rangle$ is a *superboson* [cf. Eq. (10)] with n excitations on the first site. The data (symbols) match the amplitudes of the localized version of a coherent state defined in Eq. (17) well, with $\alpha' = 1.5e^{1.42i}$ (continuous and dashed line).

Analogously, we perform the same analysis considering as initial state a cat state $|C\rangle$ on site $j=0$. Indeed, since the phase factor $e^{if\,(s,U,T)}$ does not depend on α, given a cat state

$$|C\rangle \bigotimes_{j>1} |0\rangle_j = \frac{1}{\mathcal{N}} \left(|\alpha\rangle_0 + e^{i\phi}|-\alpha\rangle_0\right) \bigotimes_{j>1} |0\rangle_j, \tag{18}$$

where $\mathcal{N}$ is a normalization constant, its localized version is

$$|\widetilde{\mathcal{C}}\rangle = \frac{1}{\mathcal{N}} \left(|\widetilde{\alpha'}\rangle + e^{i\phi}|-\widetilde{\alpha'}\rangle\right), \tag{19}$$

where $|\widetilde{\mathcal{C}}\rangle \equiv \mathcal{U}(s,U)|C\rangle$ and $\alpha' = \alpha e^{if\,(s,U,T)}$. We call $|\widetilde{\mathcal{C}}\rangle$ a *supercat* state.

We can extend Eq. (17) to states of the form

$$|\psi\rangle = |00\ldots0\rangle \otimes \left(\sum_{n=0}^{\infty} \rho_n \beta^{\theta n} |n\rangle_j\right) \otimes |00\ldots0\rangle, \tag{20}$$

where $\rho_n \in \mathbb{R}$ and $\beta, \theta \in \mathbb{C}$. Indeed, if we apply the adiabatic protocol to the state defined in Eq. (20), the phase acquired can be absorbed into β. Coherent states, cat states, and squeezed states all fall into the class described in Eq. (20). In other words, using the adiabatic protocol, not only can we engineer the localized versions of states such as coherent and squeezed states but we can do so preserving their single-mode properties.

For instance, the localized versions of coherent and squeezed states can be implemented either via the adiabatic time evolution or the application of an operator $\mathcal{M}$ that is linear or quadratic in the superbosonic operators $\mathcal{A}$. The operator $\mathcal{M}$ can be obtained applying the adiabatic protocol to its single-site counterpart M, namely $\mathcal{M} = \mathcal{U}(s,U)M\mathcal{U}(s,U)^\dagger$. For instance, we define the dressed displacement operator,

$$\mathcal{D}(\alpha) = \exp\left(\alpha\mathcal{A}^\dagger - \alpha^*\mathcal{A}\right), \tag{21}$$

where $\alpha \in \mathbb{C}$ is the displacement parameter, and the dressed squeezed operator,

$$\mathcal{S}(\xi) = \exp\left[\frac{1}{2}\left(\zeta^*\mathcal{A}^2 - \text{h.c.}\right)\right], \tag{22}$$

where $\zeta \in \mathbb{C}$ is the squeezing parameter, the action of which on the vacuum creates a *supercoherent* and *supersqueezed* state, respectively. However, the most natural

way to prepare such states is by starting from their single-mode version and then adiabatically turning on the off-diagonal term $\propto e^{-s}$ in the Hamiltonian. Note that these states are Gaussian with respect to the *superbosonic* operators $\mathcal{A}^{(\dagger)}$ and not with respect to the bare operators $\hat{a}^{(\dagger)}$. We call these states *super-Gaussian*.

We find that *superbosons* $|\widetilde{n}_0\rangle$, with different n_0 and the same position j of the first nonvacant site, are connected via the operators $\mathcal{A}_j^{(\dagger)}$. We see that their localized feature makes their energies approximately evenly spaced as a function of n_0 (cf. Appendix B). The evenly spaced energies of different ground states and the fact that the different ground states are connected via a bosonic operator $\mathcal{A}_j(s,U)^{(\dagger)}$ resemble the features of a quadratic Hamiltonian, such as the one-dimensional harmonic oscillator. Adding up these properties, the action of the interacting Hamiltonian $H(s,U)$ in Eq. (1) in the manifold of the ground states is approximatively equivalent to a free theory in the *superbosonic* operators $\mathcal{A}_j(s,U)^{(\dagger)}$, namely

$$H(s,U) \approx \sum_{j=-\infty}^{+\infty} \epsilon_0 \mathcal{A}_j(s,U)^\dagger \mathcal{A}_j(s,U), \tag{23}$$

the eigenstates of which are $\bigotimes_{j=-\infty}^{+\infty}(\mathcal{A}_j(s,U)^\dagger)^{k_j}|0\rangle$, where $k_j \in [0,\infty)$. The effective Hamiltonian in Eq. (23) captures the action of the full Hamiltonian Eq. (1) on a *superboson* $|\widetilde{n}\rangle$ well up to a certain n that is parametrically large in s and U, since corrections to the evenly spaced feature of the ground-states energies become important as n increases. Moreover, the effective Hamiltonian in Eq. (23) neglects the interaction between neighboring *superbosons*. Therefore, in the infinite set of eigenstates of Eq. (23), only those given by *superbosons* separated by a large number of empty sites with respect to the typical localization length ξ approximate eigenstates of the original model well (up to corrections that are exponentially small with the distance of two *superbosons*). For instance, the state $\mathcal{A}_1(s,U)^\dagger \mathcal{A}_{j\gg\xi}(s,U)^\dagger|0\rangle$, which describes two far-localized excitations, is an eigenstate of the effective theory in Eq. (23) and, approximately, of the original Hamiltonian in Eq. (1). Instead, the state $\mathcal{A}_1(s,U)^\dagger \mathcal{A}_2(s,U)^\dagger|0\rangle$, which describes two nearly localized excitations, is an eigenstate of Eq. (23) with energy $2\epsilon_0$, while it is not an eigenstate of the original model in Eq. (1), since we are neglecting the contribution coming from the interacting part of the Hamiltonian. Despite these limitations, the effective Hamiltonian in Eq. (23) captures the equilibrium properties in the localized phase and the dynamical features of states such as the *supercat* state and the *supersqueezed* state well when the interacting part between *superbosons* can be neglected. In this regard, the properties of the localized phase of quantum East models are reminiscent of the l-bit construction in MBL [61–64].

Let us consider a *supercat* state $|\psi(t=0)\rangle = |\widetilde{\mathcal{C}}\rangle$ defined in Eq. (19) as an initial state in order to test the effective quadratic theory in Eq. (23). We evolve it and compute the fidelity

$$\mathcal{F}(t) = |\langle\psi(t)|\psi(t=0)\rangle|^2. \tag{24}$$

As shown in Fig. 8, the fidelity displays almost perfect oscillations at short times, followed by a drop and almost perfect revivals. The short-time behavior is compatible with a rotation of the *supercat* state in the *dressed* phase space $\tilde{X}_0 = (\mathcal{A}_0 + \mathcal{A}_0^\dagger)$ and $\tilde{P}_0 = -i(\mathcal{A}_0 - \mathcal{A}_0^\dagger)$, as expected from the effective Hamiltonian in Eq. (23). We can approximately compute the dynamics of the *supercat* state $|\widetilde{\mathcal{C}}\rangle$ generated by Eq. (23) as

$$e^{-iHt}|\widetilde{\mathcal{C}}\rangle \approx \frac{1}{\mathcal{N}}\Big(|\widetilde{\alpha}(t)\rangle + e^{i\phi}|-\widetilde{\alpha}(t)\rangle\Big), \tag{25}$$

where $\alpha(t) = \alpha(t=0)e^{-i\epsilon_0 t}$. The state in Eq. (25) is a rotating *supercat* state in the *dressed* space. From Eq. (25), we can estimate the expected fidelity. In Fig. 8, we compare the expected value and the numerical results. The former matches the numerical results up to times parametrically large in s and $1/\alpha$. On the one hand, nonlinear corrections are suppressed the more the system is localized. On the other, corrections to the linear dependence of the energies $\langle\widetilde{n}|\hat{H}|\widetilde{n}\rangle$ become important the larger n is or, equivalently, α, leading to dephasing processes [93]. The revivals can be explained considering nonlinear effects; indeed, perfect revivals are observed for single-mode cat states with self-Kerr interaction [94] (for a circuit-QED implementation, see Ref. [95]). Differently from the latter case, we have an extended state and nearest-neighbor density-density interactions. As a consequence, pushing the simulations to longer times we observe no perfect revivals as in the case of single bosonic modes with Kerr nonlinearities. Such behavior might be captured by improving the effective theory introduced in Eq. (23), adding nonlinearities in the basis of *superbosonic* degrees of freedom. This is beyond our current scope and therefore left as a potential interesting follow-up.

We can extend these dynamical properties to any state prepared via the adiabatic protocol starting from a state of the form given in Eq. (20). Indeed, these states evolve analogously to the *supercat* state under the effective quadratic theory defined in Eq. (23). The *super-Gaussian* states fall into this class. Once again, we highlight that these states are Gaussian with respect to the *superbosonic* operators $\mathcal{A}^{(\dagger)}$ but not with respect to the bare operators $\hat{a}^{(\dagger)}$.

We have discussed the application of the adiabatic protocol to a single-site state embedded in the vacuum; however, this extends directly to more general initial states. For instance, we could have started from a product state made of single-body states separated by a large number of empty sites, with respect to the localization length ξ, or from a superposition of those. At the end of the protocol, each one

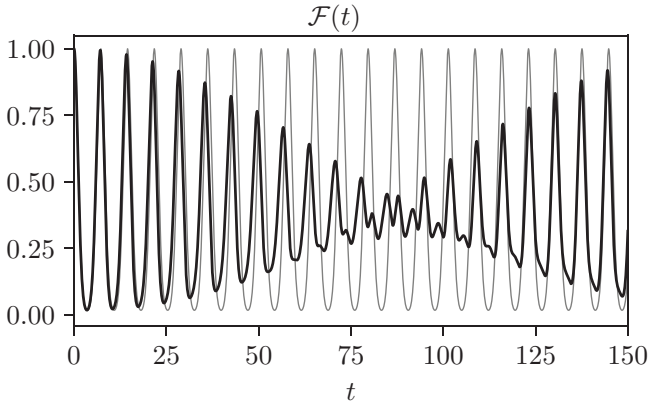

FIG. 8. The coherent dynamics of a *supercat* state with $\alpha = 1.5$. We simulate a system of size $L = 15$. We fix $s = 1$ and $U = 1$. We show the dynamics of the fidelity $\mathcal{F}$ (dark black line). The light black line is the expected value from the effective quadratic theory in Eq. (23) with a numerically extracted $\epsilon_0 \approx 0.43$.

will be dressed independently of the others. Therefore, the final state will be made of localized states concatenated one after the other.

V. EFFECTS OF DEPHASING AND LOSSES

In this section, we investigate the dynamical properties of the localized states introduced in Sec. IV when coupled to the environment. Here, we study the effects of two different couplings with an external bath, namely a global dephasing due to a noise coupled to the local densities, which commutes with the "East" symmetry, and global losses, which break the "East" symmetry. Both of these couplings are experimentally relevant in superconducting-circuit setups [71], which are at the core of the experimental implementation we propose in Sec. VI. We provide numerical evidence that local information is erased very slowly when the environment is coupled via densities to the system. We show how the characteristic time scales depend on the parameters of the Hamiltonian, the initial state, and the strength of the coupling to the environment. On the contrary, we show that losses are highly disruptive and that the time scales are dependent on the strength of the coupling to the environment and the initial state, while the underlying coherent dynamics does not play a substantial role. At the end of the section, we show that the typical couplings to the environment currently achieved in superconducting circuits are small enough to make the effects of the coherent dynamics appreciable and observable in the presence of losses.

We consider the following Linbland master equation:

$$\dot{\hat{\rho}} = -i[\hat{H}, \hat{\rho}] + \gamma \sum_j \left(\hat{L}_j \hat{\rho} \hat{L}_j^\dagger - \frac{1}{2} \left\{ \hat{L}_j^\dagger \hat{L}_j, \hat{\rho} \right\} \right), \quad (26)$$

where $\hat{\rho}$ is the state of the system, $\hat{H}$ is the Hamiltonian in Eq. (1) with $\epsilon = 0$, $\hat{L}_j$ is the quantum jump operator acting on site j, and γ is the corresponding rate. In order to efficiently simulate the Lindbland master equation in Eq. (26), we resort to the quantum trajectories algorithm, which is based on defining the effective non-Hermitian Hamiltonian

$$\hat{H}_{\text{eff}} = \hat{H} - i\frac{\gamma}{2} \sum_j \hat{L}_j^\dagger \hat{L}_j, \quad (27)$$

and alternating the action of the Hamiltonian given in Eq. (27) with the jump operators $\{\hat{L}_j\}$ based on a stochastic process (for the details, we refer to Refs. [96,97]). The dynamics of any observable $\hat{\mathcal{O}}$ result from averaging over N different uncorrelated stochastic trajectories labeled by $\eta \in [1, N]$,

$$\langle \hat{\mathcal{O}}(t) \rangle = \left\langle \mathcal{O}_\eta(t) \right\rangle_\eta, \quad \mathcal{O}_\eta(t) = {}_\eta\langle \psi(t) | \hat{\mathcal{O}} | \psi(t) \rangle_\eta, \quad (28)$$

where $|\psi(t)\rangle_\eta$ is the state for a given stochastic trajectory $\eta \in [1, N]$ at time t and $\langle \cdot \rangle_\eta$ denotes the average over the different trajectories. We resort to tensor-network methods for performing the simulations (see Appendix E). We consider two different jump operators, namely $\hat{L}_j = \hat{n}_j$ and $\hat{L}_j = \hat{a}_j$. The former corresponds to dephasing, while the latter corresponds to losses. We choose such jump operators in order to investigate the effects of the environment when it preserves the "East" symmetry, as for the dephasing process, or when it does not, as for the global losses. Both situations are relevant in superconducting-circuit setups [71]. We compute the observables averaging over 1000–3000 stochastic realizations depending on the value of γ and the jump operator.

We study the dynamical properties of *superbosons* $|\widetilde{n}\rangle$ defined in Eq. (10), since they constitute the building blocks of any localized state that we can engineer. Then, we turn our attention to a paradigmatic superposition of *superbosons*, namely the *supercat* state, providing arguments to extend our findings to a class of states to which *supersqueezed* and *supercoherent* states belong. We consider as initial state $|\psi_k(t=0)\rangle = \bigotimes_{j=-\infty}^{k-1} |0\rangle_j \otimes |\widetilde{n}\rangle$, where the subscript k in $|\psi_k(t=0)\rangle$ refers to the position of the first site of the embedded *superboson*. Since $|\widetilde{n}\rangle$ is localized with localization length ξ [cf. Eq. (6)], we can truncate its support to $L' \gg \xi$ sites. Thus, our initial state is

$$|\psi_k(t=0)\rangle = |0\rangle_j^{\otimes_{j=-\infty}^{k-1}} \otimes |\widetilde{n}\rangle_{L'} \otimes |0\rangle_j^{\otimes_{j=k+L'}^{+\infty}}, \quad (29)$$

where L' is the size of the *superboson* support.

In a generic nonintegrable system, we expect information about initial states encoded in local observables to be washed out fast. Here, we want to study how localization and slow dynamics instead protect the information

encoded in local quantities. We compute the fidelity and the imbalance. The fidelity [cf. Eq. (24)] provides global information about the state and sets an upper bound on the time dependence of the expectation value of any local observable. Nonetheless, the fidelity is highly sensitive to any local perturbation of the state. Indeed, it is enough to have even a single occupied site far from the superbosons $|\widetilde{n}\rangle$ to make Eq. (24) negligibly small. Among all the possible local observables, we want to investigate if the initial localized peak remains well resolved. We therefore compute the imbalance between the occupation of the initial peak and the second highest peak in the system, namely

$$\mathcal{I} = \frac{n_k - \max_{j\neq k} n_j}{n_k + \max_{j\neq k} n_j}, \tag{30}$$

where k is the position of the first site of the embedded state [cf. Eq. (29)]. The imbalance $\mathcal{I} \in [-1, 1]$ and for $\mathcal{I} > 0$ the initial peak is the largest one in the system.

When dissipation enters in the form of a dephasing noise coupled to the bosonic densities, the Lindbland equation respects the "East" symmetry. The jump operators commute with the operator in Eq. (3). Thus, the n excitations at the first site of the *superbosons* $|\widetilde{n}\rangle$ and the empty sites to its left are conserved. Furthermore, since the the jump operators are not able to generate excitations out of the vacuum and the state is exponentially localized, we can keep only a few empty sites to the left of $|\widetilde{n}\rangle_{L'}$ without introducing relevant size effects. For the set of parameters that we choose, restricting the *superboson* support to $L' \approx 10$ sites and keeping only one empty site to its right turns out to be sufficient. Thus, our initial state is

$$|\psi(t=0)\rangle = |\widetilde{n}_0\rangle_{L'} \otimes |0\rangle. \tag{31}$$

In Fig. 9, we show the dynamics of the fidelity and imbalance for different values of s and noise strength γ keeping $U = 1$, starting from the state in Eq. (31) with $n_0 = 1$. The imbalance displays an exponential decay $\mathcal{I}(t) \sim \mathcal{I}(0)e^{-t/\tau}$, with τ dependent on the initial state, the parameters of the Hamiltonian, and the coupling strength γ with the external bath. The decay time τ increases the more the system is in the localized phase and the larger is the initial occupation n_0, while it decreases with the noise strength γ as $\tau \propto 1/\gamma$. Therefore, the time decay τ can be enhanced by either tuning the parameters of the Hamiltonian or embedding a *superboson* with n_0 large [cf. Eq. (31)]. On the one hand, increasing s or U helps to protect the local memory at longer times, at the cost of making the initial state less entangled. Indeed, in the $s, U \to \infty$ limit, the Hamiltonian tends to $\propto \sum_i (U n_i n_{i+1} + n_i)$, the ground state of which is a product state of eigenstates of number operators. On the other hand, we can exploit the bosonic nature of the system and embed a *superboson* with a larger initial n_0, keeping s small and enhancing the initial state entanglement. It is important to stress that despite the exponential

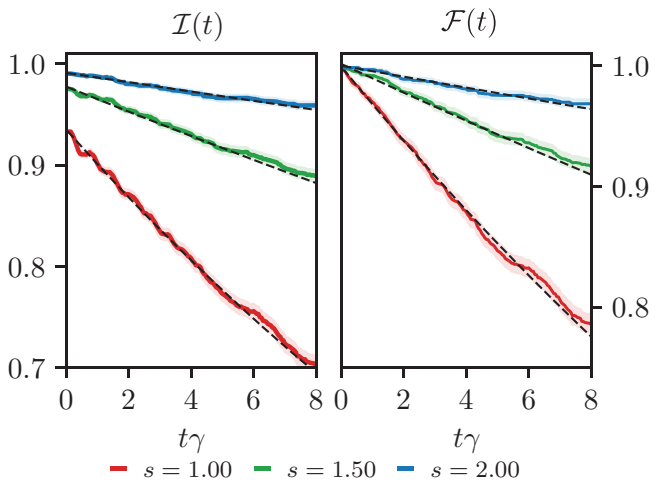

FIG. 9. The time evolution of the imbalance [cf. Eq. (30)] and fidelity [cf. Eq. (24)] starting from the state in Eq. (31) and subjected to the dissipative dynamics given by Eq. (26) with quantum jump operator $\hat{L}_j = \hat{n}_j$. We fix $n_0 = 1$, $U = 1$, and $\gamma = 0.1$ and we swipe across different values of $s \in [1, 2]$. The initial value $\mathcal{I}(0)$ ranges from approximately 0.93 to approximately 0.99 as s increases. We show results for $s = \{1, 1.5, 2\}$, on top of which we plot the exponential fit (dashed black line). Both plots are in linear-linear scale. The light area surrounding the curves represents the statistical error due to the finite number of sampled trajectories.

feature of the decay, the time scale τ is generally very large with respect to the time scales of the coherent dynamics of the system. From Eq. (30), and inspecting the late-times average occupation number, the initial peak remains still well resolved and so does the information encoded within it.

The fidelity decays exponentially fast in time $\mathcal{F}(t) \sim e^{-t/\tau'}$, with a decoherence time τ' dependent on the parameters of the Hamiltonian, the initial state, and the strength of the noise. Analogously to the decay time τ of the imbalance, the decoherence time τ' increases the more the system is in the localized phase and decreases with the noise strength γ as $\tau' \propto 1/\gamma$. Contrary to the imbalance, the fidelity drops faster the larger is n_0. Indeed, the conserved initial occupation n_0 pumps excitations on the next site, reducing the typical coherent time scales by approximately $1/(n_0 e^{-s})$ and effectively enhancing the effects of the environment.

Under the action of single-body losses, the dynamics no longer preserve the "East" symmetry. Indeed, losses can deplete the occupation of the first site, which fixes the "East" symmetry sector.

Since the vacuum is invariant under the action of losses and coherent dynamics cannot create excitations to the West of the initial embedded *superboson*, we can still consider Eq. (31) as our initial state. In Fig. 10, we show the dynamics of the fidelity and imbalance for different values of n_0, keeping $U = 1$, $s = 1.5$, and $\gamma = 0.1$ fixed. Losses

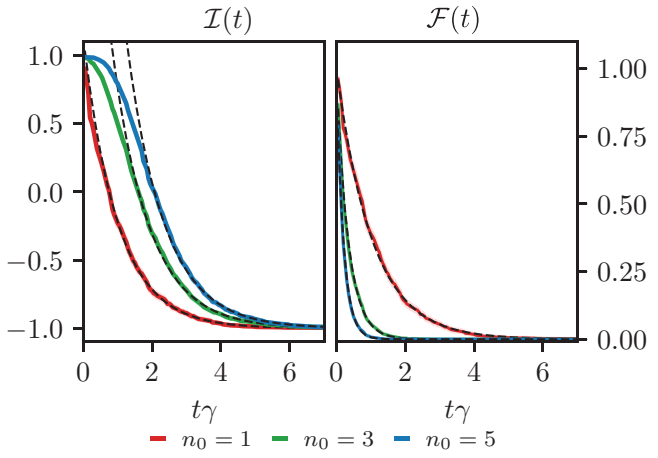

FIG. 10. The time evolution of the imbalance [cf. Eq. (30)] and fidelity [cf. Eq. (24)] starting from the state in Eq. (31), with $n_0 \in \{1, 3, 5\}$, and subjected to the dissipative dynamics given by Eq. (26) with quantum jump operator $\hat{L}_j = \hat{a}_j$. We fix $U = 1$, $s = 1.50$ ($e^{-s} \approx 0.22$), and $\gamma = 0.1$. The imbalance initial value is $\mathcal{I}(0) \approx 0.99$. In the main figures, we show results for three different values of $n_0 = \{1, 3, 5\}$, on top of which we plot the exponential fit (dashed black line). The imbalance and fidelity decay as an exponential (the dashed lines are the associated fits). Both plots are in linear-linear scale. The light area surrounding the curves represents the statistical error due to the finite number of sampled trajectories.

turn out to be detrimental to the initial state independent of the parameters of the Hamiltonian. Instead, the height of the initial peak plays a substantial role in enhancing the conservation of the imbalance. Intuitively, if the first site n_0 is highly occupied at time $t = 0$, it will require longer times to drain all the particles. This leads to an initial *plateaux* in the imbalance, followed by an exponential decay toward the minimum value $\mathcal{I}(t \to \infty) = -1$. The decay is well fitted by $\mathcal{I}(t) = \left(Ae^{-t/\tau} - 1\right)$ at long times, where $\tau \propto 1/\gamma$ is the relaxation time and A is a constant. The insensitivity of the time decay with respect to the parameters of the Hamiltonian indicates that the slow dynamics does not provide additional protection against this type of coupling to the environment. Indeed, the decay of the imbalance is due to the emission of particles from the first occupied site, which fixes the symmetry sector, and since the coherent dynamics cannot create excitations on top of it the initial peak is depleted in time $\propto 1/\gamma$.

The fidelity drops to zero exponentially fast, as expected, with a decay time that is parametrically small in the occupation of the initial peak. Indeed, the higher the peak is, the larger is the probability that the emission occurs, which immediately produces a state orthogonal to the initial one.

Despite losses being more detrimental with respect to dephasing, we show at the end of the section that the coherent dynamics takes place on time scales that are small with respect to the relaxation time in typical superconducting circuits (cf. Sec. VI for the experimental implementation of the bosonic quantum East model).

Note that we can immediately extend our analysis to a large variety of states. For instance, we can consider states given by the superposition of *superbosons* embedded in different regions of the systems, namely

$$|\Psi\rangle \propto |\psi_k(t=0)\rangle + e^{i\theta}|\psi_s(t=0)\rangle, \tag{32}$$

where $|\psi_k(t=0)\rangle$ is defined in Eq. (29), θ is a phase, and $|s-k| \gg \xi$. These two states are weakly coupled by the coherent and dissipative dynamics. In a first approximation, we can apply our analysis to each of them separately and therefore predict their dynamics easily.

The extension of these results to superposition of *superbosons* embedded in the same support [cf. Eq. (15)] is less trivial and depends on the specific coupling to the environment. For instance, a coupling that does not preserve the "East" symmetry makes the different states dynamically connected, likely leading to different results from the ones observed for the single *superbosons*. On the other hand, a coupling that preserves the "East" symmetry can also lead to additional phenomena such as dephasing processes between the superimposed states. Indeed, we observe that coupling to the densities is also detrimental. We give further details in Sec. V A, exploring the effects of local dephasing in the system.

A. Local dephasing

We now investigate the effects of local dephasing in the dynamical properties of a state given by the superposition of *superbosons* embedded in the same support. Among the possible choices, we consider a paradigmatic *super-Gaussian* state, namely the *supercat* state, and then we generalize.

We consider local dephasing due to noise coupled to the densities (see, e.g., Ref. [98]). In the case of local dephasing acting on a compact support $\mathcal{S}$, the effective theory in Eq. (27) turns into

$$\hat{H}_{\text{eff}} = \hat{H} - i\frac{\gamma}{2}\sum_{j\in\mathcal{S}} \hat{L}_j^\dagger \hat{L}_j, \tag{33}$$

where the summation is along the support $\mathcal{S}$. We consider $\hat{L}_j = \hat{n}_j$ as the jump operator.

We study the impact of the dephasing as a function of the strength γ and the extension of its support $\mathcal{S}$. Since the dephasing preserves the "East" symmetry, we can once again focus on a system comprising a few sites without introducing relevant finite-size effects. We initialize our system in the state

$$|\psi(t=0)\rangle = |\widetilde{\mathcal{C}}\rangle_L, \tag{34}$$

where $|\widetilde{\mathcal{C}}\rangle_L$ is a *supercat* state [cf. Eq. (19)] with support L and average number of particles $|\alpha|^2$. A support

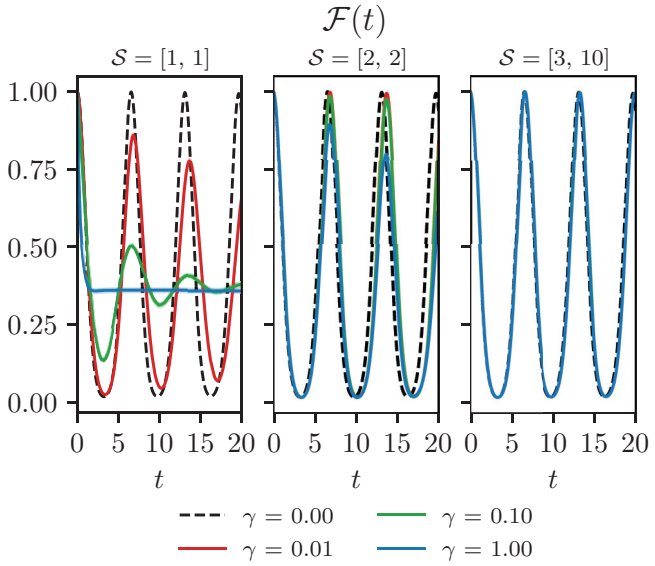

FIG. 11. The dynamics of the fidelity [cf. Eq. (24)] of a *supercat* state with $\alpha = 1.5$ upon changing the noise strength γ and its support $\mathcal{S} = [a, b]$, starting from site a and ending at site b. We fix $U = 1$ and $s = 1.5$. The initial state is exponentially localized around the site $j = 1$. The dephasing is highly disruptive only in an exponentially localized region around the peak (see the first two columns). Instead, if it acts on a region far from the localized peak, it does not produce any appreciable effect at the scale shown in the plots. The light area surrounding the curves represents the statistical error due to the finite number of sampled trajectories.

of $L = 10$ turns out to be large enough for the parameters explored ($\alpha = 1.50$, $s = 1.5$, and $U = 1$). In Fig. 11, we show the dynamics of the fidelity as a function of the coupling strength γ and support $\mathcal{S}$. The *supercat* state is still localized in space for any γ and $\mathcal{S}$. Nonetheless, the coherence of the state is highly dependent on γ and $\mathcal{S}$. Indeed, local dephasing is highly disruptive in an exponentially localized region around the peak, where the state is mostly located. If, instead, the local dephasing acts on a region far from the localized peak, it does not produce any appreciable effect. More precisely, we estimate that the typical time τ at which the embedded state is appreciably affected by the noise scales as $\tau \sim \min_{|k-j|\in\mathcal{S}} 1/(\gamma\langle n_j\rangle) \sim \min_{|k-j|\in\mathcal{S}} e^{|k-j|/\xi}/\gamma$, where k is the site where the peak is located. We numerically verify the polynomial dependence of τ on γ. On the contrary, it is not possible to extract the dependence on the support $\mathcal{S}$ with high enough accuracy from the times explored, because of the slowness of the decay.

Our findings can be extended to other channels that do not necessarily preserve the "East" symmetry. For instance, losses acting far from the localized peak will not affect local information encoded in the localized state. Furthermore, we expect that the observed dynamical properties can be easily extended to any state prepared via the adiabatic protocol from a state of the form given in Eq. (20), to which *super-Gaussian* states belong.

In this section, we have discussed the effects of dephasing and losses, without much emphasis on the actual value of the coupling strength γ to the environment in typical superconducting circuits (cf. Sec. VI for the implementation). As previously mentioned, we set the on-site bare frequency of bosons as our energy scale, which is $\mathcal{O}$(GHz) in typical superconducting circuits [71]. The typical strength of the coupling to the environment γ is $\mathcal{O}$(MHz) [71]. Therefore, $\gamma \approx 10^{-3}$ in our dimensionless units. As a consequence, coherent dynamics take place on smaller scales with respect to the operational times of typical superconducting platforms of $\mathcal{O}(1\ \mu\text{s})$, hinting that the physics of localized states is potentially observable in state-of-the-art experiments. Corroboration of this statement with more quantitative calculations would require an *ab initio* study of the dynamics of the architecture introduced in Sec. VI, which constitutes an interesting follow-up project *per se*.

VI. SUPERCONDUCTING-CIRCUIT IMPLEMENTATION

In this section, we propose an experimental implementation of the Hamiltonian in Eq. (1) in terms of a simple superconducting-circuit setup. We consider a chain of driven superconducting qubits. A superconducting qubit is basically a quantized LC oscillator with capacitance C and nonlinear inductance L [71]. This nonlinear dependence can be achieved via a Josephson junction working in the superconducting regime without introducing undesired dissipative effects [71,99,100]. In particular, we consider here the SNAIL introduced in Ref. [81] as our building block. We consider specifically the SNAIL parameters in Ref. [101], where kinetically constrained terms (at just two sites) are obtained using the second-order nonlinearity $\propto (\hat{a}^\dagger\hat{a}^\dagger a + \text{h.c.})$ of the SNAILs. Differently from Ref. [101], we do not use the second-order nonlinearity of SNAILs. Indeed, any superconducting qubit that can be approximated as an anharmonic oscillator with positive anharmonicity could be a suitable candidate for our setup (e.g., the C-shunt flux qubit [102]).

We consider an array of L driven superconducting (SC) qubits coupled via an exchange interaction as our starting point. We retain all the energy levels of each SC qubit. The Hamiltonian can be decomposed as a sum of three terms, $H = H_0 + H_{\text{drive}} + V$, where

$$\begin{aligned} H_0 &= \sum_{j=1}^{L} \omega_j \hat{a}_j^\dagger \hat{a}_j + \frac{E_C}{2} \hat{a}_j^\dagger \hat{a}_j^\dagger \hat{a}_j \hat{a}_j, \\ H_{\text{drive}} &= \sum_{j=1}^{L-1} e^{-i\alpha_j t} \left(\Omega_j \hat{a}_j^\dagger + \epsilon_{j+1} \hat{a}_{j+1}^\dagger\right) + \text{h.c.}, \\ V &= \sum_{j=1}^{L-1} g \left(\hat{a}_j \hat{a}_{j+1}^\dagger + \text{h.c.}\right), \end{aligned} \tag{35}$$

where $\hat{a}_j^\dagger$ ($\hat{a}_j$) creates (destroys) an excitation in the jth SC qubit; H_0 is the bare Hamiltonian of the SC qubits with qubit frequencies $\{\omega_j\}_{j=1}^L$ and anharmonicity $E_C > 0$ [71]; H_{drive} describes the action of classical drive fields on the bare SC qubits; and V describes hopping processes that can be engineered by a common bus resonator [103] or a direct capacitance [104]. An illustration of the scheme of Eq. (35) is given in Fig. 1(a).

We work in the weak-coupling regime, $g \ll |\omega_j - \omega_{j+1}|$, and in the low-anharmonicity limit, $E_C \ll |\omega_j - \omega_{j+1}|$, for all j. The former condition is necessary in order to have far-detuned processes connected by V and therefore to treat V in perturbation theory [105]. The low-anharmonicity limit is necessary to retrieve a bosonic model in the effective perturbative Hamiltonian achieved after treating V with a Schrieffer-Wolf (SW) transformation in the small-g limit. Each SC qubit $j \in [1, L-1]$ is driven by a classical drive field of amplitude Ω_j and frequency α_j. These classical drive fields give rise to the desired interaction together with undesired single-site fields in the low-energy effective Hamiltonian [106]. In order to get rid of them, we add another drive field on each SC qubit $j \in [2, L]$ of amplitude ϵ_j and frequency α_{j-1} [107,108].

We are interested in exploiting the multilevel (bosonic) structure of SC qubits. We do not reduce each component of the system to a qubit. We therefore introduce the ladder operators

$$\hat{a}_j = \sum_{\ell=0}^{\infty} \sqrt{\ell+1}\,|\ell, j\rangle\langle \ell+1, j| \equiv \sum_{\ell=0}^{\infty} \hat{c}_{\ell,j}, \tag{36}$$

where $\hat{c}_{\ell,j}$ is the ladder operator that destroys an excitation in the $(\ell+1)$th level and creates an excitation in the ℓth level on the jth SC qubit. Analogously, we can define its Hermitian conjugate, $\hat{c}_{\ell,j}^\dagger$.

We work in the dispersive regime, $g \ll \Delta_{j,j+1}$, where $\Delta_{i,j} = \omega_i - \omega_j$. We perturbatively diagonalize the Hamiltonian $H_0 + V$ to second order in g via a SW transformation S [109]. The drive-field terms in H_{drive} are modified by the same SW transformation. From now on, we neglect terms of order $\mathcal{O}(g^2\Omega_j/\Delta_{j,j+1}^2)$ and higher. We move to the frame that rotates at the frequencies of the drives and we neglect the fast-oscillating terms by employing the rotating-wave approximation (RWA). Before detailing the calculations, we discuss the physics of each term in the Hamiltonian defined in Eq. (35). The bare Hamiltonian H_0 provides the necessary anharmonicity that we desire. The perturbation V gives rise to the nearest-neighbor interaction, a renormalization of the bare energies of the SC qubits, and some additional two-excitation processes. The drive field yields the constrained terms $\hat{n}_j(\hat{a}_{j\pm1} + \hat{a}_{j\pm1}^\dagger)$ toward "East" and "West." The time dependence of the drive fields in the laboratory frame enables us to get rid of the undesired processes, such as the two-excitation processes and the "West" terms, passing in the rotating frame of the drive fields and employing the RWA.

In order to find the explicit form of the SW transformation, we follow the prescription in Ref. [110]. First, we compute $\eta = [H_0, V]$; we consider η with arbitrary coefficients as an ansatz for S. Finally, we fix these coefficients, imposing the condition $[S, H_0] = -V$. We obtain (cf. Appendix F 1)

$$S = \sum_{j=1}^{L-1} \sum_{\ell,s=0}^{\infty} \frac{g}{\tilde{\Delta}_{\ell,j+1} - \tilde{\Delta}_{s,j}} \left(\hat{c}_{s,j}\hat{c}_{\ell,j+1}^\dagger - \hat{c}_{s,j}^\dagger \hat{c}_{\ell,j+1}\right), \tag{37}$$

where $\tilde{\Delta}_{\ell,j} = (\omega_j + E_C\ell)$: the first summation is along the system, while the second summation is along all the levels of the SC qubits. Using the Baker-Campbell-Hausdorff expansion, the Hamiltonian in Eq. (1) after the SW transformation reads

$$\begin{aligned}\tilde{H} &\equiv e^S H e^{-S} \\ &\approx H_0 + H_{\text{drive}} + [S, H_{\text{drive}}] + \frac{1}{2}[S, V] + \mathcal{O}\left(\frac{g^2\Omega}{\Delta^2}\right).\end{aligned} \tag{38}$$

After lengthy yet standard calculations, we obtain $\tilde{H}$ explicitly dependent on the ladder operators $\hat{c}_{\ell,j}^{(\dagger)}$ introduced in Eq. (36) and with coefficients dependent on the site and internal levels (see Appendix F 2). Our aim is to write $\tilde{H}$ as a function of the bosonic operators $\hat{a}_j^{(\dagger)}$. We need to find a regime in which the coefficients in $\tilde{H}$ are approximately independent of the specific level, so that we can use Eq. (36). These coefficients are similar to the one appearing in Eq. (37). In order to make them level independent, we need

$$\tilde{\Delta}_{\ell,j+1} - \tilde{\Delta}_{s,j} \approx \omega_{j+1} - \omega_j \equiv \Delta_{j+1,j}, \tag{39}$$

which holds if $|\ell - s| \ll |\Delta_{j+1,j}|/E_C$. Since the SC qubit can have an infinite number of excitations, we have $(\ell - s) \in (-\infty, +\infty)$. This means that Eq. (39) cannot be satisfied for all possible ℓ and s if $E_C \neq 0$. Nonetheless, it can be achieved up to a certain value N of ℓ and s, such that $N \ll |\Delta_{j+1,j}/E_C|$. Therefore, the coefficients in $\tilde{H}$ satisfy Eq. (39) up to the Nth energy level, leading to a bosonic Hamiltonian that approximates the action of the full Hamiltonian to states with an occupation that is small with respect to N (cf. Appendix F 3). The bosonic $\tilde{H}$ still displays undesired processes, such as hopping and local fields. We move to a rotating frame of reference via the unitary transformation

$$U = \exp\left(it \sum_{j=1}^{L-1} \alpha_j \hat{n}_{j+1}\right) \tag{40}$$

and we neglect all the oscillating terms by employing the RWA (cf. Appendix F 4). In doing so, we get rid of almost all the undesired processes except for some local fields at the sites $j \geq 2$. These fields can be eliminated via the additional drive fields of amplitudes $\{\epsilon_j\}$, analogously to what has been done in similar scenarios (see, e.g., Refs. [107,108]). We tune their amplitudes such that they cancel the undesired local terms. We obtain the matching condition $\epsilon_j = g\Omega_{j-1}/\Delta_{j-1,j}$, with $j \geq 2$. This leads to the effective Hamiltonian

$$\tilde{H} = \sum_{j=1}^{L} \tilde{\omega}_j \hat{n}_j + \frac{E_C}{2}\hat{n}_j\hat{n}_j + \frac{2g^2 E_C}{\Delta_{j,j+1}^2}\hat{n}_j\hat{n}_{j+1} + \frac{g\Omega_j E_C}{\Delta_{j,j+1}^2}\hat{n}_j\left(\hat{a}_{j+1}^\dagger + \hat{a}_{j+1}\right) \quad (41)$$

where $\tilde{\omega}_1 = \omega_1 - E_C/2 + \mathcal{O}(g^2/\Delta_{12})$ and $\tilde{\omega}_{j\neq 1} = \omega_j - E_C/2 - \alpha_{j-1} + \mathcal{O}(g^2/\Delta_{j,j+1})$.

We now evaluate the couplings in Eq. (41), considering the SNAIL as our SC qubit and using the parameters of Ref. [101]. We work in the parameter regime in which the SNAILs Hamiltonian is given by H_0 in Eq. (35). We fix $E_C \approx 150$ MHz, $g = 75$ MHz and $\omega_j \approx 3$ GHz. We consider the classical drive fields with amplitude $\Omega_j = -100$ MHz (the amplitude has to be negative to have the correct sign for the constrained hopping), which can be achieved by adding a π phase to the external drive fields. Any real system is inevitably coupled to the environment and SC circuits are no exception. In the context of SC circuits, two different time scales are defined, namely T_1 and T_2 [71]. The time scale T_1 is the typical time at which the coupling with the environment leads excited states to decay to lower-energy states. The time scale T_2 quantifies the coherence time of the system. For consistency with the chosen parameters (taken from Ref. [101]), we also consider, as T_1 and T_2, the values from Ref. [101], which are $T_{1,2} \approx 1$ μs. We fix the qubit frequencies ω_j and the drive-field frequencies α_j in order to satisfy: (i) the dispersive regime, valid for $g/\Delta_{j,j+1} \ll 1$; (ii) the low-anharmonicity limit, $E_C \ll \Delta_{j,j+1}$; (iii) the validity of the RWA, namely $|\alpha_j| \gg \Omega_j$, $|\alpha_{j+1} - \alpha_j| \gg \Omega_j$ and $|\alpha_{j+2} - \alpha_j| > g\Omega_{j+2}/\Delta_{j+1,j+2}$; (iv) $\tilde{\omega}_j \approx \omega_j - \alpha_{j-1} > 0$ for $j > 1$, necessary in order to have localization; (v) $1/T_{1,2}$ small with respect to the typical energies in the effective Hamiltonian in Eq. (41); and (vi) that the system is in the localized phase.

The more stringent conditions are given by (ii) and (v). A good trade-off between (ii) and (v) is obtained at $|\Delta_{j,j+1}| \equiv \Delta \approx 5E_C \approx 750$ MHz, for which the typical time scale of the kinetically constrained term is approximately $T_{1,2}/2$. We have $g/\Delta_{j,j+1} \approx 0.1$, meaning that (i) is reasonably satisfied. Condition (iii) is satisfied by a staggered configuration of the drive fields with an additional dishomogeneity between next-neighbor drive-field frequencies the third condition in (iii), for instance: $\alpha_j = \alpha_{j-1} + (-1)^j(\delta + (j-1)\zeta)$ for $j \in [2,4]$ and boundary condition $\alpha_1 \gg \Omega$ (for larger systems, it is enough to periodically repeat the configuration of the frequencies), with $\delta \gg \Omega$, $\alpha_1 \gg \Omega$, and $\zeta \gg g\Omega/\Delta \approx 10$ MHz. Condition (iv) is satisfied by a staggered configuration of the qubit frequencies as well: $\omega_{j+1} = \omega_j + (-1)^j\Delta$ for $j \geq 2$, $\omega_2 = \omega_1 + \Delta$, with boundary condition $\omega_1 > \alpha_1$. For instance, we can consider $\alpha_1 = 750$ MHz, $\delta = 750$ MHz, $\zeta = 10$ MHz, and $\omega_1 = 3$ GHz. These conditions lead to Eq. (41) being almost translationally invariant (except for dishomogeneities in the frequencies $\tilde{\omega}_j$ of the order of approximately 5%, which can be eliminated via a more fine-tuned choice of $\{\omega_j\}$). Moreover, condition (vi) is satisfied for this set of parameters. In Table I, we summarize a possible set of parameters available in state-of-the-art superconducting circuits for implementing the bosonic quantum East model.

TABLE I. A possible configuration for the external classical drive-field frequencies $\{\alpha_j\}$ and bare frequency $\{\omega_j\}$ of SNAILs for the experimental implementation of the bosonic quantum East model in a system of size $L = 5$. For bigger system sizes, it is enough to periodically repeat the configuration from site $j = 2$ to $j = 5$. The other parameters are as follows: anharmonicity $E_C = 150$ MHz, bare capacitive coupling $g = 75$ MHz, and classical drive-field amplitude $\Omega = -100$ MHz.

	$j=1$	$j=2$	$j=3$	$j=4$	$j=5$
α_j (GHz)	0.75	1.6	0.65	1.7	0.75
ω_j (GHz)	3	3.75	4.5	3.75	4.5

VII. PERSPECTIVES

The implementation of a kinetically constrained East model using superconducting circuits represents a bridge between the two communities of circuit-QED and nonergodic quantum dynamics. It has the potential to attract the former toward fundamental questions regarding dynamical phase transitions and to stimulate the latter toward the search for quantum-information and metrological applications of constrained dynamics. Our explicit construction of localized analogs of squeezed and cat states relying on the East constraint represents a first stepping stone in this direction.

A fruitful prosecution of this work is the study of an analog of the mobility edge separating localized from delocalized states in the spectrum of East models (for the mobility edge in MBL, see Refs. [20,21]). An understanding of how such a mobility edge scales with Λ is essential for predicting the onset of dynamical transitions in platforms with unidirectional constraints, as well as of practical interest. For instance, a mobility edge at finite energy density is a feature of direct relevance for experimental realizations, since it would yield the conditions

for performing efficient quantum manipulations deep in the localized phase when finite-temperature or heating effects are present. A related interesting question is the survival of the effective integrable description of the localized phase discussed in Sec. IV upon increasing the density of energy above the ground state. This would have implications for heat- and particle-transport features of the East model in the nonergodic phase, which would be governed by the effective integrable description in Eq. (23), as happens for MBL systems [111].

The insensitivity to noise acting away from localized peaks could open up a path toward the study of the protection of spatially separated macroscopic superpositions of superbosonic states. Given the slow decay of localized wave packets in the presence of noise, one could conceive the storage and noise resilience of long-lived many-body entangled states in faraway regions, with applications to quantum communication.

To conclude, we observe that the implementation discussed in Sec. IV may be easily adapted to retain kinetic terms with both East and West symmetries. This could, for instance, lead to the formation of localized modes at edges of the wire, with exciting perspectives for novel forms of topological states in kinetically constrained models that are realizable with circuit QED. We are currently focusing our research efforts in this direction.

VIII. ACKNOWLEDGMENTS

We are indebted to S. M. Girvin for careful proofreading of the manuscript and for providing valuable comments. We thank Mari Carmen Bañuls and Juan P. Garrahan for insightful discussions. This project has been supported by the Deutsche Forschungsgemeinschaft (DFG, German Research Foundation) through the Project ID 429529648—TRR 306 QuCoLiMa ("Quantum Cooperativity of Light and Matter"), and the grant HADEQUAM- MA7003/3-1; and by the Dynamics and Topology Center, funded by the State of Rhineland Palatinate. Parts of this research were conducted using the Mogon supercomputer and/or advisory services offered by Johannes Gutenberg University Mainz [112], which is a member of the Alliance for High Performance Computing in Rhineland Palatinate (AHRP [113]), and the Gauss Alliance e.V. We gratefully acknowledge the computing time granted on the Mogon supercomputer at Johannes Gutenberg University Mainz [112] through the project "DysQCorr."

APPENDIX A: ROLE OF ON-SITE DENSITY-DENSITY INTERACTION

In the main text, we focus on a simplified version of the model without on-site density-density interactions, to keep to a minimum the amount of technical details in the course of the presentation. In the following, we address the role of on-site density-density interactions, focusing on the localization properties of the ground state and comparing with the statements in the main text resulting from numerics performed at $U > 0$ and $\epsilon = 0$.

Starting from the Hamiltonian in Eq. (5), we consider $U = 0$ and $\epsilon \geq 0$. For $\epsilon = 0$, the model does not display localization at finite s in the bosonic limit, as extensively discussed in Sec. III. On the other hand, for $\epsilon > 0$, the ground state is localized for $s > s_c$ in the bosonic limit, with s_c being parametrically small in ϵ. We perform the same scaling analysis as a function of the cutoff Λ discussed in Sec. III. In Fig. 12, we show the inverse of the localization length ξ swiping s for different values of Λ at fixed ϵ. The scaling analysis suggests that the transition point $s_c(\Lambda, \epsilon)$ converges to a finite value independent of Λ for $\Lambda \to \infty$. The overall qualitative picture is therefore unaffected if one considers on-site or nearest-neighbor nonlinearities.

A nonzero value of ϵ introduces, however, anharmonic spacings between ground states with different values of n_0. Indeed, we have, for the energy of the ground state, $E(n_0) \approx n_0/2 + \epsilon n_0^2/2$. This additional anharmonicity has an impact on the adiabatic protocol discussed in Sec. IV, since each adiabatically evolved state $\mathcal{U}|n_0\rangle_0 \otimes \bigotimes_{j>0} |0\rangle_j$ in Eq. (15) would acquire a phase with a nonlinear dependence in n_0, which technically complicates state preparation without altering the main physical message. Nonetheless, it is still possible to tame the effect of this nonlinearity by considering a small enough ϵ, at the cost

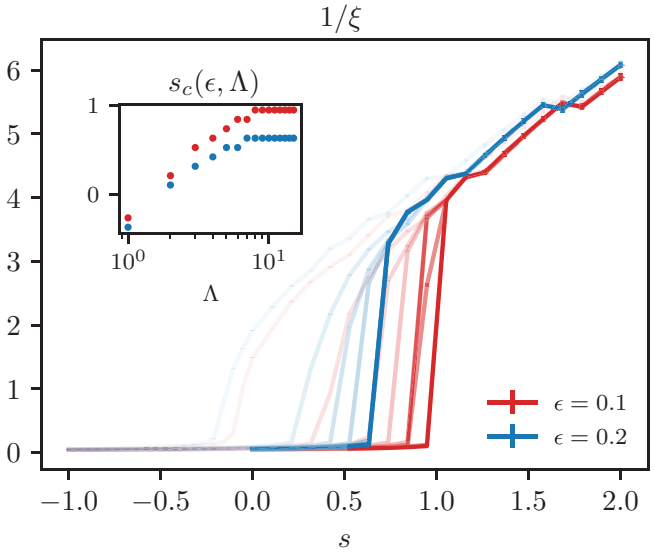

FIG. 12. The inverse of the localization length ξ in a system of $L = 15$ "active" sites in the symmetry sector $n_0 = 1$, $\beta_{r=0}$. The main plot shows the inverse of the localization length ξ^{-1} as a function of s for different values of $\Lambda \in [1, 15]$ and ϵ at $U = 0$. The darker lines correspond to larger values of Λ. The inset shows the behavior of $s_c(\epsilon, \Lambda)$ as a function of Λ for $\epsilon = 0.1$ (red) and $\epsilon = 0.2$ (blue) at $U = 0$.

of having a smaller e^{-s} (larger s) and therefore working effectively deeper in the localized phase. These types of unnecessary technical complications are at the root of our choice of working throughout the main text with $\epsilon = 0$ and $U > 0$.

APPENDIX B: PROPERTIES OF THE LOCALIZED GROUND STATE UPON CHANGING n_0

In this appendix, we discuss the properties of the ground state upon changing the symmetry sector specified by the occupation n_0 of the first nonempty site. We show that the transition point and the exponential decaying tail of the ground-state occupation are weakly dependent on n_0. We discuss the dependence of the ground-state energy on n_0, which is relevant in the state preparation via the adiabatic protocol discussed in Sec. IV.

We perform the same scaling analysis as a function of the cutoff Λ discussed in Sec. III (see Fig. 13). We extract the transition point s_c for different values of n_0 from the inverse of the localization length ξ. The existence of a finite critical point s_c in the $\Lambda \to \infty$ limit turns out to be weakly dependent on the specific symmetry sector n_0 at fixed U. We investigate the dependence of the localized tail of the ground state $|\psi_0(n_0)\rangle$ as a function of n_0 (we exclude the first site, which fixes the symmetry). To this end, we compute $|\langle\psi_0(n_0 = 1)|\psi_0(n_0)\rangle|^2$, with $n_0 \geq 1$ (see Fig. 14). We fix $n_0 = 1$ as a reference since we want to see whether or not the tail is weakly dependent on n_0. All the ground states are computed by fixing $\Lambda = 30$. The overlap $|\langle\psi_0(n_0)|\psi_0(n_0 = 1)\rangle|$ strongly depends on s and U. Indeed, the more the system is in the localized phase, the more the exponentially localized tail is weakly dependent on n_0. Therefore, deep in the localized phase, $|\psi_0(n_0)\rangle$ is approximately independent of the specific sector n_0 and we can write

$$|\widetilde{n_0}\rangle \equiv |n_0\rangle \otimes |\psi_0(n_0)\rangle \approx |n_0\rangle \otimes |\psi_0\rangle, \tag{B1}$$

where $|\psi_0\rangle$ is explicitly independent of n_0.

The weak dependence of $|\psi_0(n_0)\rangle$ with respect to n_0 has consequences for the ground-state energies. Indeed, the expectation value of the Hamiltonian on Eq. (B1) is

$$E_0(n_0) \equiv \langle\widetilde{n_0}|\hat{H}|\widetilde{n_0}\rangle \approx \frac{1}{2}n_0 + \mathcal{O}(n_0 e^{-1/\xi(n_0)}), \tag{B2}$$

where $\langle\hat{n}_j\rangle \sim e^{-j/\xi(n_0)}$ since we are in the localized phase. In Fig. 15, we give numerical evidence of Eq. (B2).

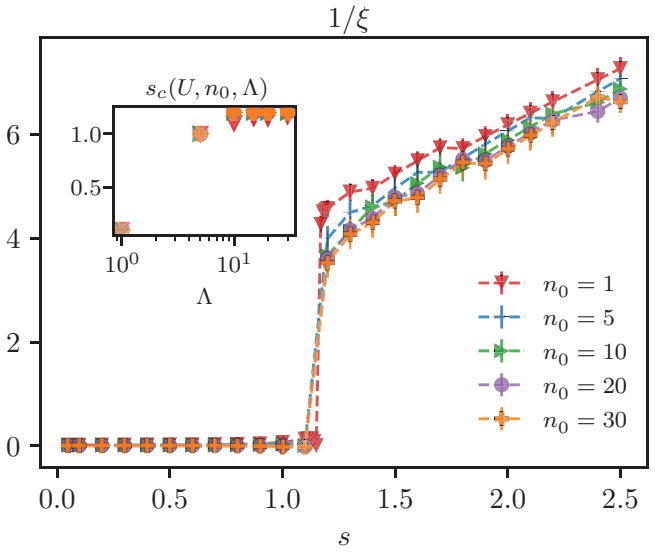

FIG. 13. The inverse of the localization length ξ in a system of $L = 15$ "active" sites upon changing s for different values of $n_0 = 1$. We fix $U = 0.1$. The main plot shows the inverse of the localization length ξ^{-1} as a function of s for $\Lambda = 30$. The inset shows the behavior of s_c as a function of Λ for different values of n_0. The circles correspond to numerically extracted values from DMRG results. The points are indistinguishable upon changing n_0 for $\Lambda \gtrsim 10$.

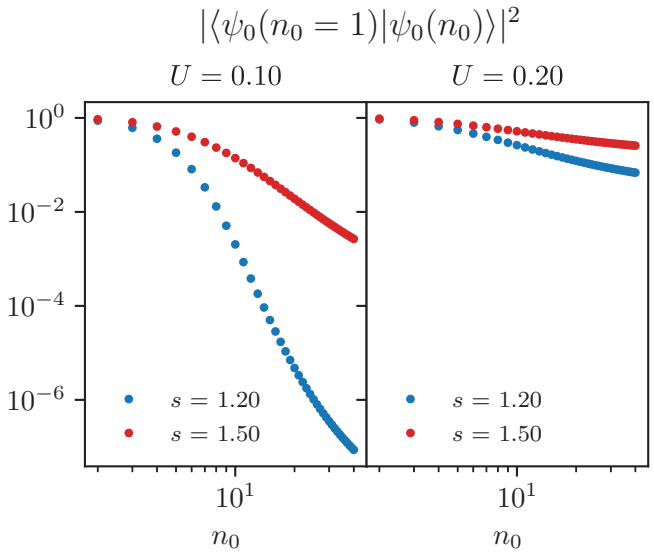

FIG. 14. The overlap of the exponential tail as a function of $n_0 \in [2, 40]$ for two different values of $U = \{0.1, 0.2\}$ and $s = \{1.20, 1.50\}$. We choose these values of U and s since we are not so deep in the localized phase. The more the system is within the localized phase, the more the localized tails are weakly dependent on n_0.

APPENDIX C: SCALING ANALYSIS IN Λ

In the main text, we show that the bosonic system displays a delocalized-localized transition at finite s if $U > 0$. Here, we show that the ground state is not only localized but is weakly dependent on the physical cutoff Λ. This provides quantitative proof that we can investigate the bosonic system with a finite Λ in the localized phase.

We fix the symmetry sector n_0 and $(s > s_c(U), U > 0)$ in the localized phase. We compute $|\psi_0(\Lambda)\rangle$ for different

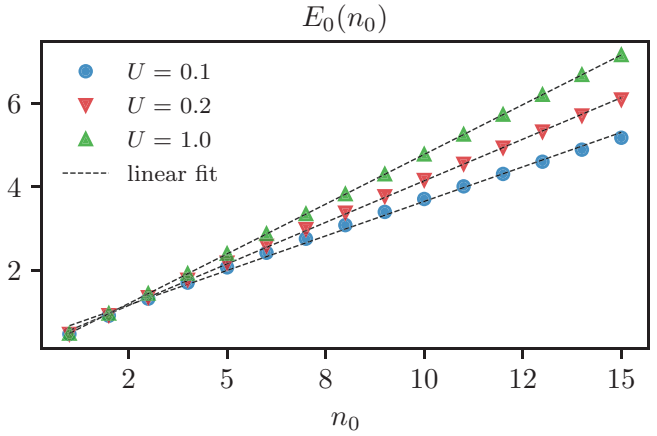

FIG. 15. The energies of the ground state as a function of n_0 for different values of U at fixed $s = 1.5 > s_c(U)$ and cutoff $\Lambda = 15$. The dashed lines are the linear fit. The more we are deep in the localized phase, the more $E(n_0) \propto n_0$.

values of Λ. We calculate $1 - |\langle\psi_0(\Lambda)|\psi_0(\Lambda+1)\rangle|^2$ as a function of Λ (see Fig. 16). The fidelity $|\langle\psi_0(\Lambda)|\psi_0(\Lambda+1)\rangle|^2$ approaches 1 exponentially fast in Λ. The more the system is in the localized phase and n_0 is small, the faster is the convergence. This gives the first evidence that the ground state of the actual bosonic system is well described with small effective cutoffs.

We compute the variance of the Hamiltonian given in Eq. (1) over the ground state $|n_0\rangle_0 \otimes |\psi_0(\Lambda)\rangle$, taking into account the bosonic nature of the original Hamiltonian in Eq. (1). This quantity is exactly zero if the state

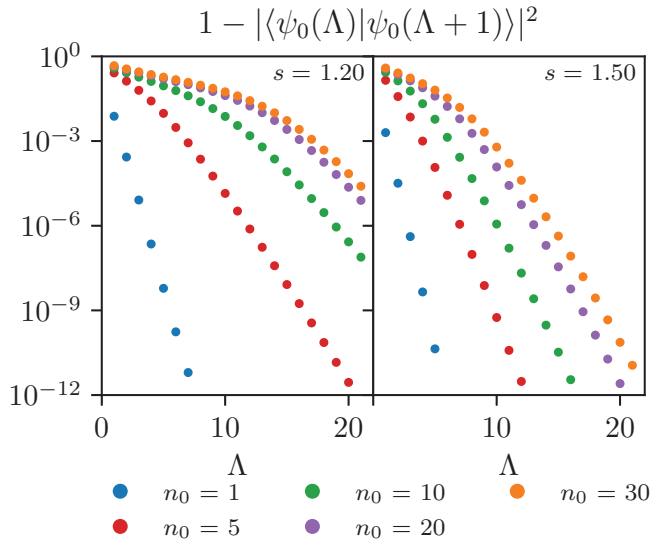

FIG. 16. The scaling analysis of $1 - |\langle\psi_0(\Lambda)|\psi_0(\Lambda+1)\rangle|$ as a function of Λ at fixed $U = 0.1$ and $s = \{1.2, 1.5\}$ for different values of $n_0 \in [1, 30]$. The dots and squares refers to the numerical results obtained at $s = 1.2$ and $s = 1.5$, respectively. The overlap tends exponentially fast to 1 in Λ. The decay is slower as n_0 increases at fixed s and U.

$|n_0\rangle_0 \otimes |\psi_0(\Lambda)\rangle$ is an eigenstate of H. We aim to see how this quantity goes to zero as a function of Λ. In order to do so, we write the Hamiltonian given in Eq. (1) as the sum of two terms, $H = H_- + H_+$. H_- acts on the Hilbert space spanned by states with an occupation number up to Λ, while H_+ acts on the Hilbert space spanned by states with an occupation number greater than Λ. We label the sectors on which $H_\pm$ acts nontrivially as the $\mathcal{H}_\pm$ sectors, respectively. We apply the same procedure to the number operator and the annihilation(creation) operator:

$$\begin{aligned}\hat{n} &= \sum_{k=0}^{\Lambda} k\,|k\rangle\langle k| + \sum_{k=\Lambda+1}^{\infty} k\,|k\rangle\langle k| \\ &= \hat{n}_- + \hat{n}_+, \\ \hat{a} &= \sum_{k=0}^{\Lambda} \sqrt{k}|k-1\rangle\langle k| + \sum_{k=\Lambda+1}^{\infty} \sqrt{k}|k-1\rangle\langle k| \\ &= \hat{a}_- + \hat{a}_+. \end{aligned} \tag{C1}$$

The commutator $[\hat{n}_-, \hat{n}_+] = 0$, while $[\hat{a}_-, \hat{a}_+] = \sqrt{\Lambda(\Lambda+1)}|\Lambda-1\rangle\langle\Lambda+1| \neq 0$. This is because the operators $\hat{a}_\pm^{(\dagger)}$ connect the two sectors $\mathcal{H}_\pm$. From Eq. (C1), we straightforwardly obtain the expressions for $H_\pm$:

$$H_\pm = -\frac{1}{2}\sum_i \hat{n}_{i,\pm}\Big[e^{-s}\left(\hat{a}^\dagger_{i+1,\pm} + \hat{a}_{i+1,\pm}\right) + - U\hat{n}_{i+1,\pm} - 1\Big]. \tag{C2}$$

In our numerical scheme, we fix a finite cutoff Λ. Therefore, we are computing the ground state $|\psi_0(\Lambda)\rangle$ of H_-. Since $\hat{a}_\pm$ are noncommuting operators, the two Hamiltonians H_- and H_+ do not commute as well. Therefore, it is not ensured that $|\psi_0(\Lambda)\rangle$ is an eigenstate of the full Hamiltonian H. We compute the variance ΔH over $|\psi_0(\Lambda)\rangle$ of the Hamiltonian $H = H_- + H_+$,

$$\Delta H = \langle H_+ H_+\rangle + \langle\{H_+, H_-\}\rangle + \langle H_- H_-\rangle - \langle H\rangle^2, \tag{C3}$$

to check whether $|\psi_0(\Lambda)\rangle$ is an eigenstate of H. The terms in $H_\pm$ that preserve the sectors $\mathcal{H}_\pm$ give a zero contribution in Eq. (C3). Indeed, the ones that keep the system in the $\mathcal{H}_-$ sector give a zero contribution since $|\psi_0(\Lambda)\rangle$ is an eigenstate within this sector by definition. Instead, the ones that keep the system in the $\mathcal{H}_+$ sector trivially give zero since we do not have any occupation larger than Λ. The only contribution comes from the operators $\hat{a}_\pm^{(\dagger)}$ or, more precisely, the term $\left(\sqrt{\Lambda+1}|\Lambda+1\rangle\langle\Lambda| + \text{h.c.}\right)$, which connects the two sectors. Using Eq. (C2), we straightforwardly obtain

$$\Delta H = \Lambda\frac{e^{-2s}}{4}\sum_{j=0}^{L-1}\langle n_j^2\rangle\langle\mathcal{P}_{j+1,\Lambda}\rangle, \tag{C4}$$

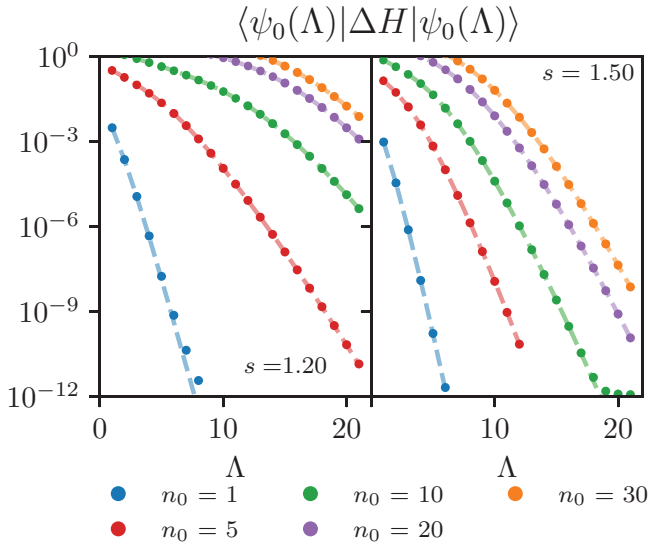

FIG. 17. The scaling analysis of $\langle\psi_0(\Lambda)|\Delta H|\psi_0(\Lambda)\rangle$ as a function of Λ at fixed $U = 0.1$ and $s = \{1.2, 1.5\}$ for different values of $n_0 \in [1, 30]$. The dots refer to the numerical results. The dashed lines are the analytical estimation given by Eq. (C4). The variance ΔH decays exponentially fast in Λ. The decay is slower as n_0 increases at fixed s and U.

where $\mathcal{P}_{j,k} = |k\rangle_{jj}\langle k|$ is the projector on the Fock state with occupation k on site j. The first term of the sum ($j = 0$) encodes the information about the fixed-symmetry sector, since $\langle\hat{n}_0^2\rangle = n_0^2$. The variance given in Eq. (C4) depends on the mean occupation number and on the projector over the Fock space on Λ. In the main text, we show that the system displays a localized phase in the bosonic limit, $\Lambda \to \infty$, if $U > 0$. This enables us to estimate Eq. (C4) in the localized phase. In the localized phase, the average occupation number of the ground state is $\langle\hat{n}_j\rangle \sim e^{-j/\xi}$ [cf. Eq. (6)]. The exponential decay of the occupation number along the chain reflects on the behavior of the expectation value of $\mathcal{P}_{k,j}$, which decays exponentially fast in k [cf. Eq. (7)]. Therefore, the series given in Eq. (C4) is finite for $\Lambda \to \infty$ and $L \to \infty$, since each term is exponentially suppressed. In Fig. 17, we numerically compute the variance ΔH over $|\psi_0(n_0, \Lambda)\rangle$ for different values of Λ and n_0. Rigorously, the cutoff Λ limits the accessible n_0, since $\langle\hat{n}_i\rangle \leq \Lambda$. Nevertheless, because n_0 appears as a constant in the Hamiltonian, we can also compute the ground state $|\psi_0(n_0, \Lambda)\rangle$ for $n_0 > \Lambda$. The numerical results match Eq. (C4) perfectly. The variance goes exponentially fast to zero. Therefore, an eigenstate of H_- is an eigenstate of the fully bosonic system as well, with a reasonably small cutoff Λ when $U > 0$.

APPENDIX D: GAUSSIANITY AND NON-GAUSSIANITY IN THE GROUND STATE

In Fig. 18, we show the correlator $\Delta_j = \langle\hat{n}_j\hat{n}_{j+1}\rangle - \langle\hat{n}_j\rangle\langle\hat{n}_{j+1}\rangle$ as a function of j for different values of s at fixed $U = 1$. We compare Δ_j computed on the ground state

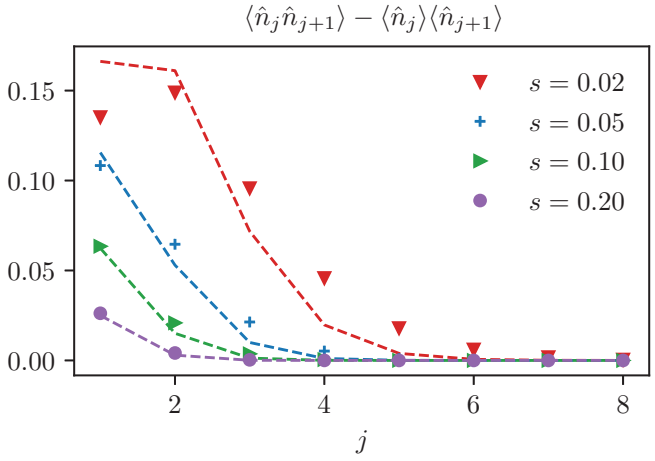

FIG. 18. The points correspond to the quantity computed on the ground state obtained via the DMRG; the continuous lines are the results obtained assuming that the state is Gaussian. We fix $U = 1$, $n_0 = 1$, and $\Lambda = 15$.

obtained via the DMRG and the one computed assuming that the same state is Gaussian in the operators $\{\hat{a}_j^{(\dagger)}\}_{j=1}^L$, which we call Δ_j^G.

APPENDIX E: NUMERICAL METHODS

In this appendix, we provide details of the parameters adopted for simulating a single stochastic trajectory at the core of the quantum trajectories method, while we refer to Ref. [96,97] for details of the algorithm. As stated in the main text, we resort to tensor networks in order to numerically integrate a single trajectory. The deterministic part of the dynamics given by the action of the effective Hamiltonian defined in Eq. (27) is performed via the time-evolving block-decimation (TEBD) algorithm with second-order Suzuki-Trotter decomposition. When a jump occurs, the corresponding jump operator is easily applied, being a single-site gate. We fix a time step $\delta t = 5 \times 10^{-3}$, a maximal bond dimension $\chi_{\max} = 75$, and we keep the singular values greater than 10^{-10}. We verify that the results are not affected by the time step δt and $\chi_{\max}$. All the simulations are performed using the ITensor library [114].

APPENDIX F: DETAILS OF SUPERCONDUCTING-CIRCUIT IMPLEMENTATION

1. Perturbative construction of the generator S of the Schrieffer-Wolff transformation

We write the Hamiltonian H_0 and the perturbation V as a function of the operators $\hat{c}_{\ell,j}^{(\dagger)}$ defined in Eq. (36):

$$H_0 = \sum_{j=1}^{L}\sum_{\ell=0}^{\infty}\omega_{\ell,j}|\ell,j\rangle\langle\ell,j| \equiv \sum_{j=1}^{L}\sum_{\ell=0}^{\infty}\omega_{\ell,j}p_{\ell,j},$$
$$V = g\sum_{j=1}^{L-1}\sum_{\ell,s=0}^{\infty}\left(c_{\ell,j}^{\dagger}c_{s,j+1} + \text{h.c.}\right), \tag{F1}$$

where $\omega_{\ell,j} = \left(\omega_j - E_C/2\right)j + E_C j^2/2$ and we introduce $p_{\ell,j} \equiv |\ell,j\rangle\langle\ell,j|$ for convenience. We compute the generator $\eta = [H_0, V]$:

$$\eta = \sum_{j=1}^{L}\sum_{\ell,s=0}^{\infty} g\left(\tilde{\Delta}_{\ell,j+1} - \tilde{\Delta}_{s,j}\right)\left(c^\dagger_{s,j}c_{\ell,j+1} - c_{s,j}c^\dagger_{\ell,j+1}\right), \tag{F2}$$

where $\tilde{\Delta}_{\ell,j} = \omega_{\ell+1,j} - \omega_{\ell,j} = (\omega_j + E_C\ell)$. Following Ref. [110], the ansatz for the generator S of the SW transformation is $S = \sum_{j=1}^{L}\sum_{\ell,s} A_{j,\ell,s}\left(c_{s,j}c^\dagger_{\ell,j+1} - c^\dagger_{s,j}c_{\ell,j+1}\right)$. We compute $[S, H_0]$ and we impose $[S, H_0] = -V$. This condition is satisfied if $A_{j,\ell,s} = g/\left(\tilde{\Delta}_{\ell,j+1} - \tilde{\Delta}_{s,j}\right)$. Therefore,

$$S = \sum_{j=1}^{L-1} S_{j,j+1}, \qquad S_{j,j+1} \equiv \sum_{\ell,s=0}^{\infty}\frac{g}{\tilde{\Delta}_{\ell,j+1} - \tilde{\Delta}_{s,j}}\left(c_{s,j}c^\dagger_{\ell,j+1} - c^\dagger_{s,j}c_{\ell,j+1}\right). \tag{F3}$$

2. Commutator of the Hamiltonian with the generator S of the Schrieffer-Wolff transformation

We write the perturbation $V = \sum_{j=1}^{L-1} V_{j,j+1}$, where $V_{j,j+1} = g\sum_{\ell,s=0}^{\infty}\left(c^\dagger_{\ell,j}c_{s,j+1} + \text{h.c.}\right)$. We compute the commutators $[S_{j-1,j}, V_{j,j+1}]$, $[S_{j,j+1}, V_{j,j+1}]$ and $[S_{j-1,j}, V_{j,j+1}]$:

$$\begin{aligned}
[S_{j,j+1}, V_{j,j+1}] &= \sum_{\ell,s}\frac{2g^2E_C}{\left(\tilde{\Delta}_{\ell+1,j+1} - \tilde{\Delta}_{s,j}\right)\left(\tilde{\Delta}_{\ell,j+1} - \tilde{\Delta}_{s+1,j}\right)}c_{s,j}c_{s+1,j}c^\dagger_{\ell+1,j+1}c^\dagger_{\ell,j+1} + \sum_{\ell,s}\frac{g^2}{\tilde{\Delta}_{\ell-1,j+1} - \tilde{\Delta}_{s,j}}\ell p_{s,j}p_{\ell,j+1} \\
&+ \sum_{\ell,s}\frac{2g^2E_C}{\left(\tilde{\Delta}_{\ell-1,j+1} - \tilde{\Delta}_{s,j}\right)\left(\tilde{\Delta}_{\ell,j+1} - \tilde{\Delta}_{s-1,j}\right)}s\ell p_{s,j}p_{\ell,j+1} - \sum_{\ell,s}\frac{g^2}{\tilde{\Delta}_{\ell,j+1} - \tilde{\Delta}_{s-1,j}}sp_{s,j}p_{\ell,j+1} + \text{h.c.}, \\
[S_{j,j+1}, V_{j-1,j}] &= \sum_{\ell,s,q}\frac{g^2E_C}{\left(\tilde{\Delta}_{\ell,j+1} - \tilde{\Delta}_{s,j}\right)\left(\tilde{\Delta}_{\ell,j+1} - \tilde{\Delta}_{s-1,j}\right)}sc_{q,j-1}p_{s,j}c^\dagger_{\ell,j+1} + \sum_{\ell,s,q}\frac{g^2}{\tilde{\Delta}_{\ell,j+1} - \tilde{\Delta}_{s,j}}c_{q,j-1}p_{s,j}c^\dagger_{\ell,j+1} + \\
&- \sum_{\ell,s,q}\frac{g^2E_C}{\left(\tilde{\Delta}_{\ell,j+1} - \tilde{\Delta}_{s,j}\right)\left(\tilde{\Delta}_{\ell,j+1} - \tilde{\Delta}_{s+1,j}\right)}c^\dagger_{q,j-1}c_{s,j}c_{s+1,j}c^\dagger_{\ell,j+1} + \text{h.c.}, \\
[S_{j-1,j}, V_{j,j+1}] &= \sum_{\ell,s,k}\frac{g^2E_C}{\left(\tilde{\Delta}_{\ell,j} - \tilde{\Delta}_{s,j}\right)\left(\tilde{\Delta}_{\ell-1,j} - \tilde{\Delta}_{s,j-1}\right)}\ell c_{s,j-1}p_{\ell,j}c^\dagger_{k,j+1} - \sum_{\ell,s,k}\frac{g^2}{\tilde{\Delta}_{\ell,j} - \tilde{\Delta}_{s,j-1}}c_{s,j-1}p_{\ell,j}c^\dagger_{k,j+1} + \\
&- \sum_{\ell,s,k}\frac{g^2E_C}{\left(\tilde{\Delta}_{\ell,j} - \tilde{\Delta}_{s,j-1}\right)\left(\tilde{\Delta}_{\ell+1,j} - \tilde{\Delta}_{s,j-1}\right)}c_{s,j-1}c^\dagger_{\ell+1,j}c^\dagger_{\ell,j}c_{k,j+1} + \text{h.c.},
\end{aligned} \tag{F4}$$

which constitute the building blocks for computing $[S, V]$. We consider a drive field acting on site j, $H_{\text{drive},j} = \Omega_j\left(e^{i\alpha_j t}a_j + \text{h.c.}\right)$. We compute the commutator $[S, H_{\text{drive},j}] = [S_{j-1,j}, H_{\text{drive},j}] + [S_{j,j+1}, H_{\text{drive},j}]$:

$$\begin{aligned}
[S_{j-1,j}, H_{\text{drive},j}] &= \sum_{\ell,s}\frac{g\Omega_jE_C}{\left(\tilde{\Delta}_{\ell-1,j} - \tilde{\Delta}_{s,j-1}\right)\left(\tilde{\Delta}_{\ell,j} - \tilde{\Delta}_{s,j-1}\right)}e^{i\alpha_j t}\ell c_{s,j-1}p_{\ell,j} - \sum_{\ell,s}\frac{g\Omega_j}{\tilde{\Delta}_{\ell,j} - \tilde{\Delta}_{s,j-1}}e^{i\alpha_j t}c_{s,j-1}p_{\ell,j} + \\
&- \sum_{\ell,s}\frac{g\Omega_jE_C}{\left(\tilde{\Delta}_{\ell+1,j} - \tilde{\Delta}_{s,j-1}\right)\left(\tilde{\Delta}_{\ell,j} - \tilde{\Delta}_{s,j-1}\right)}e^{-i\alpha_j t}c_{s,j-1}c^\dagger_{\ell+1,j}c^\dagger_{\ell,j} + \text{h.c.}, \\
[S_{j,j+1}, H_{\text{drive},j}] &= \sum_{\ell,s}\frac{g\Omega_jE_C}{\left(\tilde{\Delta}_{\ell,j+1} - \tilde{\Delta}_{s,j}\right)\left(\tilde{\Delta}_{\ell,j+1} - \tilde{\Delta}_{s+1,j}\right)}e^{-i\alpha_j t}sp_{s,j}c^\dagger_{\ell,j+1} + \sum_{\ell,s}\frac{g\Omega_j}{\tilde{\Delta}_{\ell,j+1} - \tilde{\Delta}_{s,j}}e^{-i\alpha_j t}p_{s,j}c^\dagger_{\ell,j+1} + \text{h.c.} \\
&- \sum_{\ell,s}\frac{\Omega_jgE_C}{\left(\tilde{\Delta}_{\ell,j+1} - \tilde{\Delta}_{s,j}\right)\left(\tilde{\Delta}_{\ell,j+1} - \tilde{\Delta}_{s+1,j}\right)}e^{i\alpha_j t}c_{s,j}c_{s+1,j}c^\dagger_{\ell,j+1} + \text{h.c.}
\end{aligned} \tag{F5}$$

3. Low-anharmonicity limit

In the following, we explicitly consider the results with $L = 4$ superconducting qubits for clarity. The generalization to a larger number of superconducting qubits is straightforward. We work in the limit $E_C \ll \Delta_{ij}$, such that $\tilde{\Delta}_{\ell,j+1} - \tilde{\Delta}_{s,j} \approx \Delta_{j+1,j} = \omega_{j+1} - \omega_j$. We neglect the contributions coming from the commutators of the drive fields controlled by $\{\epsilon_j\}$, since, as we show, they give subleading corrections. From Eqs. (F4) and (F5) and using the identities $\sum_{\ell=0}^{\infty} c_{\ell,j} = a_j$, $\sum_{\ell=0}^{\infty} \ell p_{\ell,j} = n_j$ and $\sum_{\ell=0}^{\infty} p_{\ell,j} = 1$, we obtain

$$
\begin{aligned}
[S,V] \approx &+\frac{2g^2E_C}{\Delta_{12}^2}a_1a_1a_2^\dagger a_2^\dagger + \frac{2g^2E_C}{\Delta_{12}^2}n_1n_2 + \frac{g^2}{\Delta_{12}}n_1 - \frac{g^2}{\Delta_{12}}n_2 + \frac{g^2E_C}{\Delta_{23}^2}a_1n_2a_3^\dagger - \frac{g^2}{\Delta_{23}}a_1a_3^\dagger - \frac{g^2E_C}{\Delta_{23}^2}a_1^\dagger a_2a_2a_3^\dagger \\
&+ \frac{g^2E_C}{\Delta_{12}^2}a_1n_2a_3^\dagger + \frac{g^2}{\Delta_{12}}a_1a_3^\dagger - \frac{g^2E_C}{\Delta_{12}^2}a_1^\dagger a_2a_2a_3^\dagger + \frac{2g^2E_C}{\Delta_{23}^2}a_2a_2a_3^\dagger a_3^\dagger + \frac{2g^2E_C}{\Delta_{23}^2}n_2n_3 + \frac{g^2}{\Delta_{23}}n_2 - \frac{g^2}{\Delta_{23}}n_3 + \text{h.c.}, \\
&+ \frac{g^2E_C}{\Delta_{34}^2}a_2n_3a_4^\dagger - \frac{g^2}{\Delta_{34}}a_2a_4^\dagger - \frac{g^2E_C}{\Delta_{34}^2}a_2^\dagger a_3a_3a_4^\dagger + \frac{g^2E_C}{\Delta_{23}^2}a_2n_3a_4^\dagger + \frac{g^2}{\Delta_{23}}a_2a_4^\dagger - \frac{g^2E_C}{\Delta_{23}^2}a_2^\dagger a_3a_3a_4^\dagger + \frac{2g^2E_C}{\Delta_{34}^2}a_3a_3a_4^\dagger a_4^\dagger \\
&+ \frac{2g^2E_C}{\Delta_{34}^2}n_3n_4 + \frac{g^2}{\Delta_{34}}n_3 - \frac{g^2}{\Delta_{34}}n_4 + \text{h.c.}, \\
[S,H_{\text{drive}}] \approx &+\frac{gE_C\Omega_1}{\Delta_{12}^2}\left\{n_1\left(e^{-i\alpha_1 t}a_2^\dagger + \text{h.c.}\right) - \left(e^{i\alpha_1 t}a_1a_1a_2^\dagger + \text{h.c.}\right)\right\} - \frac{g\Omega_1}{\Delta_{12}}\left(e^{-i\alpha_1 t}a_2^\dagger + \text{h.c.}\right) \\
&+ \frac{gE_C\Omega_2}{\Delta_{12}^2}\left\{n_2\left(e^{-i\alpha_2 t}a_1^\dagger + \text{h.c.}\right) - \left(e^{i\alpha_2 t}a_2a_2a_1^\dagger + \text{h.c.}\right)\right\} + \frac{g\Omega_2}{\Delta_{12}}\left(e^{-i\alpha_2 t}a_1^\dagger + \text{h.c.}\right) \\
&+ \frac{gE_C\Omega_2}{\Delta_{23}^2}\left\{n_2\left(e^{-i\alpha_2 t}a_3^\dagger + \text{h.c.}\right) - \left(e^{i\alpha_2 t}a_2a_2a_3^\dagger + \text{h.c.}\right)\right\} - \frac{g\Omega_2}{\Delta_{23}}\left(e^{-i\alpha_2 t}a_3^\dagger + \text{h.c.}\right) \\
&+ \frac{gE_C\Omega_3}{\Delta_{23}^2}\left\{n_3\left(e^{-i\alpha_3 t}a_2^\dagger + \text{h.c.}\right) - \left(e^{i\alpha_3 t}a_3a_3a_2^\dagger + \text{h.c.}\right)\right\} + \frac{g\Omega_3}{\Delta_{23}}\left(e^{-i\alpha_3 t}a_2^\dagger + \text{h.c.}\right) \\
&+ \frac{gE_C\Omega_3}{\Delta_{34}^2}\left\{n_3\left(e^{-i\alpha_3 t}a_4^\dagger + \text{h.c.}\right) - \left(e^{i\alpha_3 t}a_3a_3a_4^\dagger + \text{h.c.}\right)\right\} - \frac{g\Omega_3}{\Delta_{34}}\left(e^{-i\alpha_3 t}a_4^\dagger + \text{h.c.}\right). \qquad \text{(F6)}
\end{aligned}
$$

4. Rotating frame of reference

We focus again on the four superconducting qubits system (cf. Appendix F 3). We change the frame of reference via the unitary transformation $U = \exp[it(\alpha_1 n_2 + \alpha_2 n_3 + \alpha_3 n_4)]$, from which

$$
\begin{aligned}
UH_{\text{drive}}U^\dagger = &\ \Omega_1(e^{i\alpha_1 t}a_1 + \text{h.c.}) + \Omega_2(e^{i(\alpha_2-\alpha_1)t}a_2 + \text{h.c.}) + \Omega_3(e^{i(\alpha_3-\alpha_2)t}a_3 + \text{h.c.}) \\
&+ \epsilon_2(a_2 + \text{h.c.}) + \epsilon_3(a_3 + \text{h.c.}) + \epsilon_4(a_4 + \text{h.c.}) \\
U[S,V]U^\dagger \approx &+\frac{2g^2E_C}{\Delta_{12}^2}e^{2i\alpha_1 t}a_1a_1a_2^\dagger a_2^\dagger + \frac{2g^2E_C}{\Delta_{12}^2}n_1n_2 + \frac{g^2}{\Delta_{12}}n_1 - \frac{g^2}{\Delta_{12}}n_2 \\
&+ \frac{g^2E_C}{\Delta_{23}^2}e^{i\alpha_2 t}a_1n_2a_3^\dagger - \frac{g^2}{\Delta_{23}}e^{i\alpha_2 t}a_1a_3^\dagger - \frac{g^2E_C}{\Delta_{23}^2}e^{-i(2\alpha_1-\alpha_2)t}a_1^\dagger a_2a_2a_3^\dagger \\
&+ \frac{g^2E_C}{\Delta_{12}^2}e^{i\alpha_2 t}a_1n_2a_3^\dagger + \frac{g^2}{\Delta_{12}}e^{i\alpha_2 t}a_1a_3^\dagger - \frac{g^2E_C}{\Delta_{12}^2}e^{-i(2\alpha_1-\alpha_2)t}a_1^\dagger a_2a_2a_3^\dagger \\
&+ \frac{2g^2E_C}{\Delta_{23}^2}e^{-2i(\alpha_1-\alpha_2)t}a_2a_2a_3^\dagger a_3^\dagger + \frac{2g^2E_C}{\Delta_{23}^2}n_2n_3 + \frac{g^2}{\Delta_{23}}n_2 - \frac{g^2}{\Delta_{23}}n_3 \\
&+ \frac{g^2E_C}{\Delta_{34}^2}e^{i(\alpha_3-\alpha_1)t}a_2n_3a_4^\dagger - \frac{g^2}{\Delta_{34}}e^{i(\alpha_3-\alpha_1)t}a_2a_4^\dagger - \frac{g^2E_C}{\Delta_{34}^2}e^{i(\alpha_1-2\alpha_2+\alpha_3)t}a_2^\dagger a_3a_3a_4^\dagger
\end{aligned}
$$

$$+\frac{g^2E_C}{\Delta_{23}^2}e^{-i(\alpha_1-\alpha_3)t}a_2n_3a_4^\dagger-\frac{g^2}{\Delta_{23}}e^{-i(\alpha_1-\alpha_3)t}a_2a_4^\dagger+\frac{g^2E_C}{\Delta_{23}^2}e^{i(\alpha_1-2\alpha_2+\alpha_3)t}a_2^\dagger a_3a_3a_4^\dagger$$
$$+\frac{2g^2E_C}{\Delta_{34}^2}e^{-2i(\alpha_2-\alpha_3)t}a_3a_3a_4^\dagger a_4^\dagger+\frac{2g^2E_C}{\Delta_{34}^2}n_3n_4-\frac{g^2}{\Delta_{34}}n_3+\frac{g^2}{\Delta_{34}}n_4+\text{h.c.} \tag{F7}$$

$$U[S,H_{\text{drive}}]U^\dagger\approx+\frac{g\Omega_1E_C}{\Delta_{12}^2}\left\{n_1\left(a_2^\dagger+\text{h.c.}\right)-\left(e^{2i\alpha_1t}a_1a_1a_2^\dagger+\text{h.c.}\right)\right\}-\frac{g\Omega_1}{\Delta_{12}}\left(a_2^\dagger+\text{h.c.}\right)$$
$$+\frac{g\Omega_2E_C}{\Delta_{12}^2}\left\{n_2\left(e^{-i\alpha_2t}a_1^\dagger+\text{h.c.}\right)-\left(e^{i(\alpha_2-2\alpha_1)t}a_2a_2a_1^\dagger+\text{h.c.}\right)\right\}+\frac{g\Omega_2}{\Delta_{12}}\left(e^{-i\alpha_2t}a_1^\dagger+\text{h.c.}\right)$$
$$+\frac{g\Omega_2E_C}{\Delta_{23}^2}\left\{n_2\left(a_3^\dagger+\text{h.c.}\right)-\left(e^{2i(\alpha_2-\alpha_1)t}a_2a_2a_3^\dagger+\text{h.c.}\right)\right\}-\frac{g\Omega_2}{\Delta_{23}}\left(a_3^\dagger+\text{h.c.}\right)$$
$$+\frac{gE_C\Omega_3}{\Delta_{23}^2}\left\{n_3\left(e^{-i(\alpha_3-\alpha_1)t}a_2^\dagger+\text{h.c.}\right)-\left(e^{i(\alpha_3-2\alpha_2+\alpha_1)t}a_3a_3a_2^\dagger+\text{h.c.}\right)\right\}+\frac{g\Omega_3}{\Delta_{23}}\left(e^{-i(\alpha_3-\alpha_1)t}a_2^\dagger+\text{h.c.}\right)$$
$$+\frac{gE_C\Omega_3}{\Delta_{34}^2}\left\{n_3\left(a_4^\dagger+\text{h.c.}\right)-\left(e^{2i(\alpha_3-\alpha_2)t}a_3a_3a_4^\dagger+\text{h.c.}\right)\right\}-\frac{g\Omega_3}{\Delta_{34}}\left(a_4^\dagger+\text{h.c.}\right). \tag{F8}$$

We discard all the oscillating terms employing the RWA in the limits,

$$\alpha_1\gg\max\left(\Omega_1,\frac{g^2E_C}{\Delta_{12}^2},\frac{g\Omega_1E_C}{\Delta_{12}^2}\right), \tag{F9}$$
$$\alpha_2\gg\max\left(\frac{g^2}{\Delta_{12}},\frac{g^2}{\Delta_{23}},\frac{g^2E_C}{\Delta_{12}^2},\frac{g^2E_C}{\Delta_{23}^2},\frac{g\Omega_2}{\Delta_{12}}\right), \tag{F10}$$
$$|\alpha_1-\alpha_2|\gg\max\left(\Omega_2,\frac{g\Omega_2E_C}{\Delta_{23}^2},\frac{g^2E_C}{\Delta_{23}^2}\right), \tag{F11}$$
$$|\alpha_2-\alpha_3|\gg\max\left(\Omega_3,\frac{g\Omega_3E_C}{\Delta_{34}^2},\frac{g^2E_C}{\Delta_{34}^2}\right), \tag{F12}$$
$$|2\alpha_1-\alpha_2|\gg\max\left(\frac{g^2E_C}{\Delta_{23}^2},\frac{g^2E_C}{\Delta_{12}^2},\frac{g\Omega_2E_C}{\Delta_{12}^2}\right), \tag{F13}$$
$$|\alpha_3-\alpha_1|\gg\max\left(\frac{g^2E_C}{\Delta_{34}^2},\frac{g^2}{\Delta_{34}},\frac{g^2E_C}{\Delta_{23}^2},\frac{g^2}{\Delta_{23}},\frac{gE_C\Omega_3}{\Delta_{23}^2},\frac{g\Omega_3}{\Delta_{23}}\right), \tag{F14}$$
$$|\alpha_1-2\alpha_2+\alpha_3|\gg\max\left(\frac{g^2E_C}{\Delta_{34}^2},\frac{g^2E_C}{\Delta_{23}^2},\frac{gE_C\Omega_3}{\Delta_{34}^2}\right). \tag{F15}$$

which are satisfied in the dispersive regime and at the low-anharmonicity E_C limit via a staggered configuration of the drive-field frequencies with a little dishomogeneity, as discussed in Sec. VI. Discarding the oscillating terms in Eq. (F7) and Eq. (F8), we obtain

$$\tilde{H}=\sum_{j=1}^{4}\left(\tilde{\omega}_j\hat{n}_j+\frac{E_C}{2}\hat{a}_j^\dagger\hat{a}_j^\dagger\hat{a}_j\hat{a}_j\right)+\sum_{j=1}^{3}\left(\frac{2g^2E_C}{\Delta_{j,j+1}^2}\hat{n}_j\hat{n}_{j+1}+\frac{g\Omega_jE_C}{\Delta_{j,j+1}^2}\hat{n}_j\left(\hat{a}_{j+1}+\hat{a}_{j+1}^\dagger\right)\right)+\sum_{j=2}^{4}\left(\epsilon_j-\frac{g\Omega_{j-1}}{\Delta_{j-1,j}}\right)\left(a_j+a_j^\dagger\right). \tag{F16}$$

Since we do not want local fields $\propto(a_j+a_j^\dagger)$, we fix the condition $\epsilon_j=g\Omega_{j-1}/\Delta_{j-1,j}$ with $j=2,3,4$. We obtain

$$\tilde{H}=\sum_{j=1}^{4}\left(\tilde{\omega}_j\hat{n}_j+\frac{E_C}{2}\hat{a}_j^\dagger\hat{a}_j^\dagger\hat{a}_j\hat{a}_j\right)+\sum_{j=1}^{3}\left(\frac{2g^2E_C}{\Delta_{j,j+1}^2}\hat{n}_j\hat{n}_{j+1}+\frac{g\Omega_jE_C}{\Delta_{j,j+1}^2}\hat{n}_j\left(\hat{a}_{j+1}+\hat{a}_{j+1}^\dagger\right)\right). \tag{F17}$$

In the dispersive regime, the drive-field amplitudes ϵ_j are very small compared to the drive fields controlled by $\{\Omega_j\}$. Therefore, it is appropriate to neglect the contributions coming from their commutators with S. The above calculations can be straightforwardly generalized to the multisite case, since the superconducting circuits in the bulk will behave analogously to the second one in the case treated explicitly above.

[1] J. Preskill, Quantum computing in the NISQ era and beyond, Quantum **2**, 79 (2018).

[2] A. Polkovnikov, K. Sengupta, A. Silva, and M. Vengalattore, Colloquium: Nonequilibrium dynamics of closed interacting quantum systems, Rev. Mod. Phys. **83**, 863 (2011).

[3] G. Carleo, F. Becca, M. Schiró, and M. Fabrizio, Localization and glassy dynamics of many-body quantum systems, Sci. Rep. **2**, 243 (2012).

[4] E. V. H. Doggen, I. V. Gornyi, and D. G. Polyakov, Stark many-body localization: Evidence for Hilbert-space shattering, Phys. Rev. B **103**, L100202 (2021).

[5] W. De Roeck and F. Huveneers, Scenario for delocalization in translation-invariant systems, Phys. Rev. B **90**, 165137 (2014).

[6] M. Schiulaz, A. Silva, and M. Müller, Dynamics in many-body localized quantum systems without disorder, Phys. Rev. B **91**, 184202 (2015).

[7] Z. Papić, E. M. Stoudenmire, and D. A. Abanin, Many-body localization in disorder-free systems: The importance of finite-size constraints, Ann. Phys. **362**, 714 (2015).

[8] L. Barbiero, C. Menotti, A. Recati, and L. Santos, Out-of-equilibrium states and quasi-many-body localization in polar lattice gases, Phys. Rev. B **92**, 180406(R) (2015).

[9] N. Y. Yao, C. R. Laumann, J. I. Cirac, M. D. Lukin, and J. E. Moore, Quasi-Many-Body Localization in Translation-Invariant Systems, Phys. Rev. Lett. **117**, 240601 (2016).

[10] A. Smith, J. Knolle, D. L. Kovrizhin, and R. Moessner, Disorder-Free Localization, Phys. Rev. Lett. **118**, 266601 (2017).

[11] R. Mondaini, K. Mallayya, L. F. Santos, and M. Rigol, Comment on "Systematic Construction of Counterexamples to the Eigenstate Thermalization Hypothesis", Phys. Rev. Lett. **121**, 038901 (2018).

[12] M. Schulz, C. A. Hooley, R. Moessner, and F. Pollmann, Stark Many-Body Localization, Phys. Rev. Lett. **122**, 040606 (2019).

[13] E. van Nieuwenburg, Y. Baum, and G. Refael, From Bloch oscillations to many-body localization in clean interacting systems, Proc. Natl. Acad. Sci. USA **116**, 9269 (2019).

[14] N. Shiraishi and T. Mori, Shiraishi and Mori Reply, Phys. Rev. Lett. **121**, 038902 (2018).

[15] M. Kormos, M. Collura, G. Takács, and P. Calabrese, Real-time confinement following a quantum quench to a non-integrable model, Nat. Phys. **13**, 246 (2017).

[16] A. J. A. James, R. M. Konik, and N. J. Robinson, Nonthermal States Arising from Confinement in One and Two Dimensions, Phys. Rev. Lett. **122**, 130603 (2019).

[17] W. Morong, F. Liu, P. Becker, K. Collins, L. Feng, A. Kyprianidis, G. Pagano, T. You, A. Gorshkov, and C. Monroe, Observation of Stark many-body localization without disorder, (2021), arXiv preprint ArXiv:2102.07250.

[18] T. Gunawardana and B. Buča, Dynamical l-bits in Stark many-body localization, (2021), arXiv preprint ArXiv:2110.13135.

[19] B. Buca, A. Purkayastha, G. Guarnieri, M. T. Mitchison, D. Jaksch, and J. Goold, Quantum many-body attractors, (2020), arXiv preprint ArXiv:2008.11166.

[20] R. Nandkishore and D. A. Huse, Many-body localization and thermalization in quantum statistical mechanics, Annu. Rev. Condens. Matter Phys. **6**, 15 (2015).

[21] D. A. Abanin, E. Altman, I. Bloch, and M. Serbyn, Colloquium: Many-body localization, thermalization, and entanglement, Rev. Mod. Phys. **91**, 021001 (2019).

[22] F. Ritort and P. Sollich, Glassy dynamics of kinetically constrained models, Adv. Phys. **52**, 219 (2003).

[23] C. Chamon, Quantum Glassiness in Strongly Correlated Clean Systems: An Example of Topological Overprotection, Phys. Rev. Lett. **94**, 040402 (2005).

[24] J. P. Garrahan, Aspects of non-equilibrium in classical and quantum systems: Slow relaxation and glasses, dynamical large deviations, quantum non-ergodicity, and open quantum dynamics, Phys. A: Stat. Mech. Appl. **504**, 130 (2018).

[25] J. M. Hickey, S. Genway, and J. P. Garrahan, Signatures of many-body localisation in a system without disorder and the relation to a glass transition, J. Stat. Mech. **2016**, 054047 (2016).

[26] M. van Horssen, E. Levi, and J. P. Garrahan, Dynamics of many-body localization in a translation-invariant quantum glass model, Phys. Rev. B **92**, 100305(R) (2015).

[27] Z. Lan, M. van Horssen, S. Powell, and J. P. Garrahan, Quantum Slow Relaxation and Metastability due to Dynamical Constraints, Phys. Rev. Lett. **121**, 040603 (2018).

[28] J. Feldmeier, F. Pollmann, and M. Knap, Emergent Glassy Dynamics in a Quantum Dimer Model, Phys. Rev. Lett. **123**, 040601 (2019).

[29] C. Castelnovo, C. Chamon, C. Mudry, and P. Pujol, From quantum mechanics to classical statistical physics: Generalized Rokhsar-Kivelson Hamiltonians and the "stochastic matrix form" decomposition, Ann. Phys. **318**, 316 (2005).

[30] A. Prem, J. Haah, and R. Nandkishore, Glassy quantum dynamics in translation invariant fracton models, Phys. Rev. B **95**, 155133 (2017).

[31] R. M. Nandkishore and M. Hermele, Fractons, Annu. Rev. Condens. Matter Phys. **10**, 295 (2019).

[32] V. Khemani, M. Hermele, and R. Nandkishore, Localization from Hilbert space shattering: From theory to physical realizations, Phys. Rev. B **101**, 174204 (2020).

[33] P. Sala, T. Rakovszky, R. Verresen, M. Knap, and F. Pollmann, Ergodicity breaking arising from Hilbert space fragmentation in dipole-conserving Hamiltonians, Phys. Rev. X **10**, 011047 (2020).

[34] T. Rakovszky, P. Sala, R. Verresen, M. Knap, and F. Pollmann, Statistical localization: From strong fragmentation to strong edge modes, Phys. Rev. B **101**, 125126 (2020).

[35] M. Pretko, X. Chen, and Y. You, Fracton phases of matter (2020), ArXiv:2001.01722.

[36] M. Pretko and L. Radzihovsky, Fracton-Elasticity Duality, Phys. Rev. Lett. **120**, 195301 (2018).

[37] S. Scherg, T. Kohlert, P. Sala, F. Pollmann, B. H. Madhusudhana, I. Bloch, and M. Aidelsburger, Observing non-ergodicity due to kinetic constraints in tilted Fermi-Hubbard chains, Nat. Commun. **12**, 1 (2021).

[38] C. J. Turner, A. A. Michailidis, D. A. Abanin, M. Serbyn, and Z. Papić, Weak ergodicity breaking from quantum many-body scars, Nat. Phys. **14**, 745 (2018).

[39] C. J. Turner, A. A. Michailidis, D. A. Abanin, M. Serbyn, and Z. Papić, Quantum scarred eigenstates in a Rydberg atom chain: Entanglement, breakdown of thermalization, and stability to perturbations, Phys. Rev. B **98**, 155134 (2018).

[40] W. W. Ho, S. Choi, H. Pichler, and M. D. Lukin, Periodic Orbits, Entanglement, and Quantum Many-Body Scars in Constrained Models: Matrix Product State Approach, Phys. Rev. Lett. **122**, 040603 (2019).

[41] S. Ok, K. Choo, C. Mudry, C. Castelnovo, C. Chamon, and T. Neupert, Topological many-body scar states in dimensions one, two, and three, Phys. Rev. Res. **1**, 033144 (2019).

[42] M. Schecter and T. Iadecola, Weak Ergodicity Breaking and Quantum Many-Body Scars in Spin-1 *xy* Magnets, Phys. Rev. Lett. **123**, 147201 (2019).

[43] V. Khemani, C. R. Laumann, and A. Chandran, Signatures of integrability in the dynamics of Rydberg-blockaded chains, Phys. Rev. B **99**, 161101(R) (2019).

[44] A. Hudomal, I. Vasić, N. Regnault, and Z. Papić, Quantum scars of bosons with correlated hopping, Commun. Phys. **3**, 1 (2020).

[45] S. Moudgalya, N. Regnault, and B. A. Bernevig, Entanglement of exact excited states of Affleck-Kennedy-Lieb-Tasaki models: Exact results, many-body scars, and violation of the strong eigenstate thermalization hypothesis, Phys. Rev. B **98**, 235156 (2018).

[46] J. Feldmeier, P. Sala, G. De Tomasi, F. Pollmann, and M. Knap, Anomalous Diffusion in Dipole- and Higher-Moment-Conserving Systems, Phys. Rev. Lett. **125**, 245303 (2020).

[47] M. Serbyn, D. A. Abanin, and Z. Papić, Quantum many-body scars and weak breaking of ergodicity, Nat. Phys. **17**, 675 (2021).

[48] J.-Y. Desaules, A. Hudomal, C. J. Turner, and Z. Papić, Proposal for Realizing Quantum Scars in the Tilted 1D Fermi-Hubbard Model, Phys. Rev. Lett. **126**, 210601 (2021).

[49] C. J. Turner, J.-Y. Desaules, K. Bull, and Z. Papić, Correspondence principle for many-body scars in ultracold Rydberg atoms, Phys. Rev. X **11**, 021021 (2021).

[50] M. Magoni, P. P. Mazza, and I. Lesanovsky, Emergent Bloch Oscillations in a Kinetically Constrained Rydberg Spin Lattice, Phys. Rev. Lett. **126**, 103002 (2021).

[51] H. Zhao, A. Smith, F. Mintert, and J. Knolle, Orthogonal quantum many-body scars, (2021), arXiv preprint ArXiv:2102.07672.

[52] J. P. Garrahan, R. L. Jack, V. Lecomte, E. Pitard, K. van Duijvendijk, and F. van Wijland, First-order dynamical phase transition in models of glasses: An approach based on ensembles of histories, J. Phys. A: Math. Theor. **42**, 075007 (2009).

[53] P. Chleboun, A. Faggionato, and F. Martinelli, Time scale separation in the low temperature east model: Rigorous results, J. Stat. Mech. **2013**, L04001 (2013).

[54] H. Kim, M. C. Bañuls, J. I. Cirac, M. B. Hastings, and D. A. Huse, Slowest local operators in quantum spin chains, Phys. Rev. E **92**, 012128 (2015).

[55] S. Gopalakrishnan, D. A. Huse, V. Khemani, and R. Vasseur, Hydrodynamics of operator spreading and quasiparticle diffusion in interacting integrable systems, Phys. Rev. B **98**, 220303(R) (2018).

[56] S. Gopalakrishnan, Operator growth and eigenstate entanglement in an interacting integrable Floquet system, Phys. Rev. B **98**, 060302(R) (2018).

[57] M. C. Bañuls and J. P. Garrahan, Using Matrix Product States to Study the Dynamical Large Deviations of Kinetically Constrained Models, Phys. Rev. Lett. **123**, 200601 (2019).

[58] L. Causer, I. Lesanovsky, M. C. Bañuls, and J. P. Garrahan, Dynamics and large deviation transitions of the XOR-Fredrickson-Andersen kinetically constrained model, Phys. Rev. E **102**, 052132 (2020).

[59] N. Pancotti, G. Giudice, J. I. Cirac, J. P. Garrahan, and M. C. Bañuls, Quantum east model: Localization, nonthermal eigenstates, and slow dynamics, Phys. Rev. X **10**, 021051 (2020).

[60] D. F. Walls and G. J. Milburn, *Quantum Optics* (Springer Science & Business Media, Berlin, Germany, 2007).

[61] A. Chandran, I. H. Kim, G. Vidal, and D. A. Abanin, Constructing local integrals of motion in the many-body localized phase, Phys. Rev. B **91**, 085425 (2015).

[62] V. Ros, M. Müller, and A. Scardicchio, Integrals of motion in the many-body localized phase, Nucl. Phys. B **891**, 420 (2015).

[63] J. Z. Imbrie, V. Ros, and A. Scardicchio, Local integrals of motion in many-body localized systems, Ann. Phys. **529**, 1600278 (2017).

[64] D. A. Huse, R. Nandkishore, and V. Oganesyan, Phenomenology of fully many-body-localized systems, Phys. Rev. B **90**, 174202 (2014).

[65] H. P. Lüschen, P. Bordia, S. S. Hodgman, M. Schreiber, S. Sarkar, A. J. Daley, M. H. Fischer, E. Altman, I. Bloch, and U. Schneider, Signatures of many-body localization in a controlled open quantum system, Phys. Rev. X **7**, 011034 (2017).

[66] Z. Lenarčič, O. Alberton, A. Rosch, and E. Altman, Critical Behavior Near the Many-Body Localization Transition in Driven Open Systems, Phys. Rev. Lett. **125**, 116601 (2020).

[67] M. V. Medvedyeva, T. c. v. Prosen, and M. Žnidarič, Influence of dephasing on many-body localization, Phys. Rev. B **93**, 094205 (2016).

[68] R. Nandkishore, S. Gopalakrishnan, and D. A. Huse, Spectral features of a many-body-localized system weakly coupled to a bath, Phys. Rev. B **90**, 064203 (2014).

[69] R. Nandkishore and S. Gopalakrishnan, Many body localized systems weakly coupled to baths, Ann. Phys. **529**, 1600181 (2017).

[70] M. H. Fischer, M. Maksymenko, and E. Altman, Dynamics of a Many-Body-Localized System Coupled to a Bath, Phys. Rev. Lett. **116**, 160401 (2016).

[71] A. Blais, A. L. Grimsmo, S. M. Girvin, and A. Wallraff, Circuit quantum electrodynamics, Rev. Mod. Phys. **93**, 025005 (2021).

[72] A. Blais, S. M. Girvin, and W. D. Oliver, Quantum information processing and quantum optics with circuit quantum electrodynamics, Nat. Phys. **16**, 247 (2020).

[73] A. Joshi, K. Noh, and Y. Y. Gao, Quantum information processing with bosonic qubits in circuit QED, Quantum Sci. Technol. **6**, 033001 (2021).

[74] A. Eickbusch, V. Sivak, A. Z. Ding, S. S. Elder, S. R. Jha, J. Venkatraman, B. Royer, S. M. Girvin, R. J. Schoelkopf, and M. H. Devoret, Fast universal control of an oscillator with weak dispersive coupling to a qubit (2021), ArXiv:2111.06414.

[75] W.-L. Ma, S. Puri, R. J. Schoelkopf, M. H. Devoret, S. Girvin, and L. Jiang, Quantum control of bosonic modes with superconducting circuits, Sci. Bull. **66**, 1789 (2021).

[76] C.-H. Wang, K. Noh, J. Lebreuilly, S. M. Girvin, and L. Jiang, Photon-Number-Dependent Hamiltonian Engineering for Cavities, Phys. Rev. Appl. **15**, 044026 2021).

[77] C. S. Wang, J. C. Curtis, B. J. Lester, Y. Zhang, Y. Y. Gao, J. Freeze, V. S. Batista, P. H. Vaccaro, I. L. Chuang, L. Frunzio, L. Jiang, S. M. Girvin, and R. J. Schoelkopf, Efficient multiphoton sampling of molecular vibronic spectra on a superconducting bosonic processor, Phys. Rev. X **10**, 021060 (2020).

[78] A. Wallraff, D. I. Schuster, A. Blais, L. Frunzio, R.-S. Huang, J. Majer, S. Kumar, S. M. Girvin, and R. J. Schoelkopf, Strong coupling of a single photon to a superconducting qubit using circuit quantum electrodynamics, Nature **431**, 162 (2004).

[79] A. A. Houck, H. E. Türeci, and J. Koch, On-chip quantum simulation with superconducting circuits, Nat. Phys. **8**, 292 (2012).

[80] J. Koch, T. M. Yu, J. Gambetta, A. A. Houck, D. I. Schuster, J. Majer, A. Blais, M. H. Devoret, S. M. Girvin, and R. J. Schoelkopf, Charge-insensitive qubit design derived from the Cooper pair box, Phys. Rev. A **76**, 042319 (2007).

[81] N. E. Frattini, U. Vool, S. Shankar, A. Narla, K. M. Sliwa, and M. H. Devoret, 3-wave mixing Josephson dipole element, Appl. Phys. Lett. **110**, 222603 (2017).

[82] I. Carusotto, A. A. Houck, A. J. Kollár, P. Roushan, D. I. Schuster, and J. Simon, Photonic materials in circuit quantum electrodynamics, Nat. Phys. **16**, 268 (2020).

[83] Y. Yanay, J. Braumüller, S. Gustavsson, W. D. Oliver, and C. Tahan, Two-dimensional hard-core Bose-Hubbard model with superconducting qubits, npj Quantum Inf. **6**, 1 (2020).

[84] O. Mansikkamäki, S. Laine, and M. Silveri, Phases of the disordered Bose-Hubbard model with attractive interactions, Phys. Rev. B **103**, L220202 (2021).

[85] S. Schmidt and J. Koch, Circuit QED lattices: Towards quantum simulation with superconducting circuits, Ann. Phys. **525**, 395 (2013).

[86] M. H. Devoret and R. J. Schoelkopf, Superconducting circuits for quantum information: An outlook, Science **339**, 1169 (2013).

[87] P. Roushan, *et al.*, Spectroscopic signatures of localization with interacting photons in superconducting qubits, Science **358**, 1175 (2017).

[88] Y. Ye, *et al.*, Propagation and Localization of Collective Excitations on a 24-Qubit Superconducting Processor, Phys. Rev. Lett. **123**, 050502 (2019).

[89] B. Chiaro, C. Neill, A. Bohrdt, M. Filippone, F. Arute, K. Arya, R. Babbush, D. Bacon, J. Bardin, R. Barends, S. Boixo, D. Buell, B. Burkett, Y. Chen, Z. Chen, R. Collins, A. Dunsworth, E. Farhi, A. Fowler, B. Foxen, C. Gidney, M. Giustina, M. Harrigan, T. Huang, S. Isakov, E. Jeffrey, Z. Jiang, D. Kafri, K. Kechedzhi, J. Kelly, P. Klimov, A. Korotkov, F. Kostritsa, D. Landhuis, E. Lucero, J. McClean, X. Mi, A. Megrant, M. Mohseni, J. Mutus, M. McEwen, O. Naaman, M. Neeley, M. Niu, A. Petukhov, C. Quintana, N. Rubin, D. Sank, K. Satzinger, A. Vainsencher, T. White, Z. Yao, P. Yeh, A. Zalcman, V. Smelyanskiy, H. Neven, S. Gopalakrishnan, D. Abanin, M. Knap, J. Martinis, and P. Roushan, Direct measurement of non-local interactions in the many-body localized phase (2020), ArXiv:1910.06024.

[90] U. Schollwöck, The density-matrix renormalization group in the age of matrix product states, Ann. Phys. **326**, 96 (2011). january 2011 Special Issue

[91] J. Sakurai and J. Napolitano, *Modern Quantum Mechanics* (Cambridge University Press, Cambridge, England, 2017).

[92] A. Messiah, *Quantum Mechanics, Dover Books on Physics* (Dover Publications, Mineola, NY, 2014).

[93] T. Barthel and U. Schollwöck, Dephasing and the Steady State in Quantum Many-Particle Systems, Phys. Rev. Lett. **100**, 100601 (2008).

[94] B. Yurke and D. Stoler, The dynamic generation of Schrödinger cats and their detection, Phys. B+C **151**, 298 (1988).

[95] G. Kirchmair, B. Vlastakis, Z. Leghtas, S. E. Nigg, H. Paik, E. Ginossar, M. Mirrahimi, L. Frunzio, S. M. Girvin, and R. J. Schoelkopf, Observation of quantum state collapse and revival due to the single-photon Kerr effect, Nature **495**, 205 (2013).

[96] D. Jaschke, S. Montangero, and L. D. Carr, One-dimensional many-body entangled open quantum systems with tensor network methods, Quantum Sci. Technol. **4**, 013001 (2018).

[97] A. J. Daley, Quantum trajectories and open many-body quantum systems, Adv. Phys. **63**, 77 (2014).

[98] P. E. Dolgirev, J. Marino, D. Sels, and E. Demler, Non-Gaussian correlations imprinted by local dephasing in fermionic wires, Phys. Rev. B **102**, 100301(R) (2020).

[99] B. Josephson, Possible new effects in superconductive tunnelling, Phys. Lett. **1**, 251 (1962).

[100] M. Tinkham, *Introduction to Superconductivity* (Courier Corporation, Mineola, NY, 2004).

[101] A. Noguchi, A. Osada, S. Masuda, S. Kono, K. Heya, S. P. Wolski, H. Takahashi, T. Sugiyama, D. Lachance-Quirion,

and Y. Nakamura, Fast parametric two-qubit gates with suppressed residual interaction using the second-order nonlinearity of a cubic transmon, Phys. Rev. A **102**, 062408 (2020).

[102] F. Yan, S. Gustavsson, A. Kamal, J. Birenbaum, A. P. Sears, D. Hover, T. J. Gudmundsen, D. Rosenberg, G. Samach, S. Weber, J. L. Yoder, T. P. Orlando, J. Clarke, A. J. Kerman, and W. D. Oliver, The flux qubit revisited to enhance coherence and reproducibility, Nat. Commun. **7**, 1 (2016).

[103] L. DiCarlo, J. M. Chow, J. M. Gambetta, L. S. Bishop, B. R. Johnson, D. I. Schuster, J. Majer, A. Blais, L. Frunzio, S. M. Girvin, and R. J. Schoelkopf, Demonstration of two-qubit algorithms with a superconducting quantum processor, Nature **460**, 240 (2009).

[104] R. Barends, *et al.*, Superconducting quantum circuits at the surface code threshold for fault tolerance, Nature **508**, 500 (2014).

[105] A. Auerbach, *Interacting Electrons and Quantum Magnetism, Graduate Texts in Contemporary Physics* (Springer, New York, NY, 2012).

[106] E. Magesan and J. M. Gambetta, Effective Hamiltonian models of the cross-resonance gate, Phys. Rev. A **101**, 052308 (2020).

[107] S. Sheldon, E. Magesan, J. M. Chow, and J. M. Gambetta, Procedure for systematically tuning up cross-talk in the cross-resonance gate, Phys. Rev. A **93**, 060302(R) (2016).

[108] A. D. Córcoles, J. M. Gambetta, J. M. Chow, J. A. Smolin, M. Ware, J. Strand, B. L. T. Plourde, and M. Steffen, Process verification of two-qubit quantum gates by randomized benchmarking, Phys. Rev. A **87**, 030301(R) (2013).

[109] A. Blais, J. Gambetta, A. Wallraff, D. I. Schuster, S. M. Girvin, M. H. Devoret, and R. J. Schoelkopf, Quantum-information processing with circuit quantum electrodynamics, Phys. Rev. A **75**, 032329 (2007).

[110] R. U. Haq, S. S. Bharadwaj, and T. A. Wani, An explicit method for Schrieffer-Wolff transformation (2019), ArXiv:1901.08617.

[111] M. Žnidarič, A. Scardicchio, and V. K. Varma, Diffusive and Subdiffusive Spin Transport in the Ergodic Phase of a Many-Body Localizable System, Phys. Rev. Lett. **117**, 040601 (2016).

[112] https://hpc.uni-mainz.de/

[113] https://www.ahrp.info/

[114] M. Fishman, S. R. White, and E. M. Stoudenmire, The ITensor software library for tensor network calculations (2020), ArXiv:2007.14822.